A suspension of conducting particles in a magnetic field – the particle stress

V. Kumaran†

Department of Chemical Engineering, Indian Institute of Science, Bangalore 560 012, India

When a suspension of conducting particles is subjected to a shear flow, there is particle rotation due to the fluid vorticity. A conductor rotating in a uniform magnetic field experiences a torque due to eddy currents both parallel and perpendicular to the direction of rotation. Eddy currents induce a magnetic moment in a conducting particle, which disturbs the magnetic field around the particle. The effect of the Maxwell stress due to the magnetic field disturbance on the rheology of a dilute suspension is calculated in a manner similar to the Einstein viscosity for a suspension of rigid particles. The expression for the stress tensor contains three symmetric stress coefficients, and two normal stress coefficients, in addition to the three antisymmetric stress coefficients calculated in Kumaran (*J. Fluid Mech.*, vol. 871, 2019, pp. 139–185). The stress coefficients depend on the relative orientation of the vorticity and magnetic field and two dimensionless parameters, β, the product of the vorticity and current relaxation time, and Σ, the ratio of the magnetic and hydrodynamic torques. In the 'linear' approximation, where only terms linear in the particle magnetic moment are retained, the particle stress depends on two dimensionless functions. For the physically important limit $\beta \ll 1$, as well as the limit $\beta \gg 1$ and $\Sigma \gg 1$, these two functions are independent of the vorticity, and depend only on the magnetic field and material properties.

Key words: suspensions, rheology, magnetic fluids

1. Introduction

Suspended particles rotate with an angular velocity equal to one half of the fluid vorticity in a linear shear flow of a viscous suspension in the absence of external torques. Eddy currents are induced in a conducting particle rotating in a magnetic field due to Faraday's law of induction. These eddy currents result in a magnetic dipole moment at the centre of the particle in accordance with Ampere's law. The interaction of the particle magnetic moment and the imposed field results in a torque which is perpendicular to the direction of the magnetic moment and the field (Halverson & Cohen 1964; Landau, Lifshitz & Pitaevskii 2014). Due to this, the particle rotation rate is different from one half of the fluid vorticity at the particle location, and the angular velocity is determined by a balance between the hydrodynamic and magnetic torques. The torque balance procedure for determining the angular velocity and the particle torque was derived in Kumaran (2019), and the antisymmetric part of the particle stress tensor $\boldsymbol{\sigma}^p$ was calculated from

† Email address for correspondence: kumaran@iisc.ac.in

the particle torque using the relation (Batchelor 1970)

$$\boldsymbol{\sigma}^p = \frac{1}{2\,V} \sum_{i=1}^{N} \hat{\boldsymbol{\epsilon}} \cdot \boldsymbol{L}_i, \tag{1.1}$$

where $\boldsymbol{L}_i$ is the torque on particle i, N is the total number of particles, V is the total volume of the suspension and $\hat{\boldsymbol{\epsilon}}$ is the third-order Levi-Civita antisymmetric tensor. The particle stress was determined in the dilute limit, where the interactions between particles are neglected. The calculation in Kumaran (2019) was incomplete, because only the antisymmetric part of the particle stress tensor was calculated; it is not possible to calculate the symmetric part from the particle torque. Here, the complete particle stress tensor (2.3), including the symmetric and antisymmetric parts, is calculated from the Maxwell stress at the particle surface. It is verified that the antisymmetric particle force moment, calculated from (2.3), is identical to that calculated from (1.1) in Kumaran (2019). The calculation of the symmetric traceless part of the particle stress from the Maxwell stress at the particle surface in a suspension of conducting particles subjected to a magnetic field in the dilute (non-interacting) limit at low Reynolds number is the subject of the present study.

The antisymmetric stress in a suspension of conducting particles in a magnetic field is qualitatively different from the antisymmetric stress in couple-stress or Cosserat fluids (Truesdell & Toupin 1960; Mindlin & Tiersten 1962; Stokes 1966). These fluids could be subjected to a local body torque density analogous to the body force density in normal fluids, and it is necessary to augment the mass and momentum conservation equations by the angular momentum conservation equation. The analogue of the stress in the angular momentum conservation equation, called the couple stress, is expressed as a function of the gradients in the vorticity using constitutive relations analogous to Newton's law of viscosity. Structured continuum theories have been proposed (Dahler & Scriven 1963; Condiff & Dahler 1964) where the internal molecular spin could be different from the local fluid rotation rate, and this difference could give rise to an antisymmetric stress proportional to the difference between the molecular spin (angular velocity of the molecules) and one half of the vorticity. In this approach, the couple stress in the torque balance equation is related to gradients in the molecular spin.

An antisymmetric stress also plays a crucial role in the rheology of a suspension of ferromagnetic particles. Ferromagnetic particles have a permanent magnetic dipole moment, and they experience a torque under an applied magnetic field. There has been a lot of work in this area, particularly in the context of 'spin-up' flow of a ferrofluid (suspension of magnetic nanoparticles with a permanent dipole moment) in a cylinder subjected to a rotating magnetic field (Moskowitz & Rosensweig 1967; Zaitsev & Shliomis 1969; Chaves, Zahn & Rinaldi 2008). In addition to the mass and momentum densities, the density of the particle spin is an additional field used in theories of ferrofluids. In these theories, the equation for the stress tensor contains a term proportional to the curl of the difference between one half of the vorticity and the particle spin density. There is a source term in the equation of the particle spin density due to the interaction between the particle moment and the external field, and a sink due to the difference between the particle spin and one half of the fluid vorticity. The continuum description also contains a 'spin diffusion' term due to the linear relationship between the couple stress and the gradient of the angular velocity (Rosensweig 2000; Rinaldi & Zahn 2002). For macroscopic particles, simulations (Wang & Prosperetti 2001; Feng *et al.* 2006) have shown that the antisymmetric part of the stress tensor is proportional to the difference between the average particle velocity and one half of the vorticity, when an external torque is exerted on the particles.

In the case of ferrofluids, a torque is exerted on the particles due to the interaction between the permanent dipole moment of the particles and the magnetic field. In contrast, for conducting particles, there is no permanent magnetic moment. The magnetic moment due to the eddy currents generated in a particle depends on the rotation rate and the magnetic field, and there is no magnetic moment in the absence of either particle rotation or the magnetic field. Due to the torque resulting from the eddy currents and the imposed magnetic field, the angular velocity of the particles is different from one half of the fluid vorticity, but the angular velocity is in turn determined from the balance between the hydrodynamic and magnetic torques. The antisymmetric stress is due to the difference in the angular velocity of macroscopic conducting particles and the local fluid rotation rate in the low-Reynolds-number (quasi-static) limit. Consequently, there is no separate particle spin density. The stress is determined as a function of the local vorticity, magnetic field and material parameters, and it does not depend on the gradients in the vorticity.

There have been extensive studies on the rheology of magnetorheological fluids, which consist of ferromagnetic particles suspended in viscous fluids (de Vicente, Klingenberg & Hidalgo-Alvarez 2011). The particles are nanometres to micrometres in size, usually anisotropic in shape, have multiple domains and could have either a permanent magnetic dipole moment or an induced magnetic moment on application of a magnetic field. In applications such as shock-absorbers, brakes and dampers, suspensions with a relatively high volume fraction of particles are constrained to flow in a thin gap between two surfaces or in a narrow tube (Klingenberg 2001). When a magnetic field is applied across the flow, the particles align in the direction of the magnetic field, jam the gap and block the flow. A salient feature of these suspensions is the fast transition between the flowing and jammed states, within a time interval of the order of milliseconds, which enables rapid on/off switching of the flow. The flowing/jammed behaviour is controlled by the Mason number, which is the ratio of the fluid shear stress and the torque per unit volume due to the applied magnetic field. In controlled experiments in a rheometer, there is not only an increase of many orders of magnitude in the viscosity at a critical Mason number (Anupama, Kumaran & Sahoo 2018), but also a yield stress is observed at very low strain rates. The critical Mason number has been related to the Bingham number, which is the ratio of yield stress and fluid stress (Sherman, Becnel & Wereley 2015). There have been several studies on the viscosity and yield stress of particles, including formulation of constitutive relations for dilute suspensions (Jansons 1983), magnetic fibre suspensions (Kuzhir, Lopez-Lopez & Bossis 2009; Lopez-Lopez, Kuzhir & Bossis 2009) and influence of particle shape on rheology (de Vicente *et al.* 2011). Spherical particles are usually considered in particle-based models (Klingenberg & Zukoski 1990; Vagberg & Tighe 2017), and the effect of particle shape is difficult to incorporate. Exact calculations of the dynamics of single dipolar spheroids in a shear flow have revealed a rich variety in the phase portraits (Almog & Frankel 1995; Sobecki *et al.* 2018; Kumaran 2020), but these have not yet been incorporated in particle-based models for magnetorheological fluids. Since magnetorheological suspensions are usually dense, the magnetic particle–particle interaction could also be important in aligning the particles. For submicrometer particles, Brownian diffusion of the particle orientation occurs due to thermal fluctuations, and the ratio of the magnetic interaction energy and the thermal energy is also an important parameter.

There have been fewer studies on the rheology of conducting but non-ferromagnetic particles subjected to a magnetic field. In contrast to ferromagnetic particles, the magnetic permeability of these particles is almost equal to that of vacuum. However, these particles do acquire a magnetic moment only under rotation due to eddy currents that are induced in

the particles; there is no magnetic moment in the absence of rotation. When the magnetic field rotates relative to the conductor, there is an eddy current induced in the conductor due to a combination of Faraday's law of induction, $\nabla \times E = -\mu_0(\mathrm{d}H/\mathrm{d}t)$, and Ohm's law, $E = \varrho J$. Here, E and H are the electric and magnetic fields, J is the current density, μ_0 is the magnetic permeability and ϱ is the electrical resistivity. A current-carrying conductor moving in a magnetic field acquires a magnetic moment due to Ampere's law, $\nabla \times H = J + \epsilon(\partial E/\partial t)$, where ϵ is the electrical permittivity. The time derivative of the electric field in Ampere's law is usually neglected for calculating the magnetic moment, because the current relaxation time, of $O(10^{-14}\ \mathrm{s})$, is usually much smaller than the other relevant time scales. The interaction of the induced magnetic moment M with the external field H_0 results in a torque on the particle, $\mu_0(M \times H_0)$.

Moffat (1990) carried out the first studies of the force and torque on conducting particles in a magnetic field, using rotating and travelling fields as typical time-dependent fields. He showed that the force on a particle could be expressed as the sum of a lift force that is irrotational and a drag force that is solenoidal, and that there is a simple relation between the drag force and the curl of the torque on a particle. The force and torque on particles due to these fields were determined, and particle trajectories were calculated. The predicted trajectories have been compared with experiments (Bolcato *et al.* 1993).

The simpler problem of a conducting particle subjected to a simple shear flow in an imposed magnetic field was considered by Kumaran (2019) at zero Reynolds number where inertial effects are neglected, and in the dilute limit where the hydrodynamic and magnetic fields of particles do not interact. For a viscous-dominated flow, the sum of the hydrodynamic and magnetic torques on the particle is zero. The hydrodynamic torque on a particle is proportional to the difference between one half of the fluid vorticity and the particle angular velocity. The magnetic torque on a conducting particle rotating in an external magnetic field H_0, $T^m = \mu_0(M \times H_0)$, depends on the magnetic moment M which is determined by solving the equations for the current density and the magnetic field within the particle (Halverson & Cohen 1964; Landau *et al.* 2014). The moment M is necessarily perpendicular to the applied magnetic field, but it has components that are parallel and perpendicular to the $\boldsymbol{\Omega}$–H_0 plane, where $\boldsymbol{\Omega}$ is the particle angular velocity. The latter is called the 'precession' torque (Goldstein 1989), and in a simple shear flow, this results in rotation perpendicular to the plane of shear when the magnetic field and angular velocity are not perpendicular.

For the electromagnetic model, the governing equations are Faraday's law of induction, Ampere's law with the quasi-static approximation discussed earlier and Ohm's law for the relation between the current and electric field. The conductor (spherical particle or shell) is considered to have uniform electrical resistivity. The relation between the angular velocity and magnetic moment is derived in appendix A of Kumaran (2019), and so it is not repeated here. The flow is assumed to be viscous, and the hydrodynamic model is the relation between the torque and the relative angular velocity for a spherical particle, $T^h = 8\pi\eta R^3((\omega/2) - \boldsymbol{\Omega})$, where T^h is the hydrodynamic torque, η is the fluid viscosity, R is the particle radius, $\boldsymbol{\Omega}$ is the particle angular velocity and ω is the vorticity at the particle centre. The sum of the hydrodynamic and magnetic torques is set equal to zero for determining the particle angular velocity as a function of the fluid vorticity and magnetic field. From dimensional analysis, the magnetic moment M is $H_0 R^3$ times a function of the product of the angular velocity and the characteristic time scale for the current relaxation in the conductor. In the limit of zero Reynolds number, the scaled angular velocity is a function of two dimensionless parameters: $\Sigma = (\mu_0 H_0^2/4\pi\eta|\omega|)$, the ratio of the characteristic magnetic and viscous torques, and the product of the current relaxation
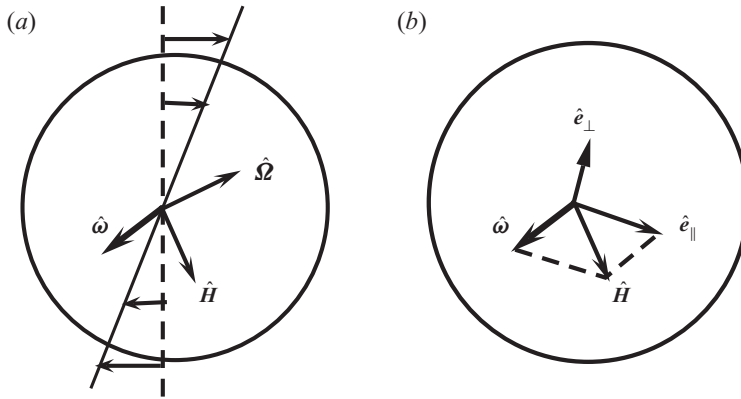
FIGURE 1. (*a*) A spherical conducting particle in a shear flow subjected to a magnetic field in the $\hat{H}$ direction experiences a rotation in the $\hat{\boldsymbol{\Omega}}$ direction; the vorticity $\hat{\boldsymbol{\omega}}$ is perpendicular to the plane of the shear. (*b*) The orthogonal coordinate system consisting of the unit vectors in the vorticity direction $\hat{\boldsymbol{\omega}}$, the unit vector $\hat{\boldsymbol{e}}_\perp$ perpendicular to $\hat{\boldsymbol{\omega}}$ in the $\hat{\boldsymbol{\omega}}$–$\hat{H}$ plane and the unit vector $\hat{\boldsymbol{e}}_\perp$ perpendicular to the $\hat{\boldsymbol{\omega}}$–$\hat{H}$ plane.

time and the vorticity, which has the form $\beta_p = (|\boldsymbol{\omega}|\mu_0 R^2/2\varrho)$ for a spherical particle and $\beta_s = (|\boldsymbol{\omega}|\mu_0 R^2\delta/2\varrho)$ for a thin shell. Here, $\boldsymbol{\omega}$ is the fluid vorticity at the particle centre, R is the particle radius, $R\delta$ is the shell thickness for a thin shell (with $\delta \ll 1$), H_0 is the applied field, μ_0 is the magnetic permeability and ϱ is the electrical resistivity. Since the magnetic torque is a nonlinear function of the particle angular velocity, the torque balance equation has to be solved iteratively to determine the angular velocity for a specified fluid vorticity and magnetic field.

The solution procedure for determining the particle angular velocity and the torque on a particle was formulated in Kumaran (2019). The antisymmetric component of the stress tensor that results from the particle torque was determined in an orthogonal coordinate system where the three unit vectors are $(\hat{\boldsymbol{\omega}}, \hat{\boldsymbol{e}}_\parallel, \hat{\boldsymbol{e}}_\perp)$ shown in figure 1(*b*), where $\hat{\boldsymbol{\omega}}$ is the unit vector along the direction of the vorticity, $\hat{\boldsymbol{e}}_\parallel = (\hat{H}-\hat{\boldsymbol{\omega}}(\hat{\boldsymbol{\omega}} \cdot \hat{H}))/\sqrt{1 - (\hat{\boldsymbol{\omega}} \cdot \hat{H})^2}$ is the unit vector perpendicular to the vorticity in the $\hat{\boldsymbol{\omega}}$–$\hat{H}$ plane and $\hat{\boldsymbol{e}}_\perp = (\hat{\boldsymbol{\omega}} \times \hat{H})/\sqrt{1 - (\hat{\boldsymbol{\omega}} \cdot \hat{H})^2}$ is the unit vector perpendicular to the $\hat{\boldsymbol{\omega}}$–$\hat{H}$ plane. The antisymmetric part of the particle stress tensor is of the form $\sigma_a^p = |\boldsymbol{\omega}|(\eta_a^{(1)}(\hat{\boldsymbol{e}}_\parallel\hat{\boldsymbol{e}}_\perp-\hat{\boldsymbol{e}}_\perp\hat{\boldsymbol{e}}_\parallel) + \eta_a^{(2)}(\hat{\boldsymbol{e}}_\perp\hat{\boldsymbol{\omega}}-\hat{\boldsymbol{\omega}}\hat{\boldsymbol{e}}_\perp) + \eta_a^{(3)}(\hat{\boldsymbol{\omega}}\hat{\boldsymbol{e}}_\parallel-\hat{\boldsymbol{e}}_\parallel\hat{\boldsymbol{\omega}}))$. The antisymmetric stress coefficients $\eta_a^{(1)}$ and $\eta_a^{(2)}$ are related due to the condition that the torque is perpendicular to the magnetic field, and the independent antisymmetric stress coefficients were evaluated in Kumaran (2019).

The present calculation consists of three parts. The first is the calculation of the particle stress as a function of the magnetic moment, the second is the calculation of the magnetic moment due to particle rotation and the third is the calculation of the angular velocity due to the balance between the hydrodynamic and magnetic torques. The second and third calculations are coupled, because the magnetic moment depends on the particle angular velocity, and the angular velocity in turn depends on the magnetic moment via the magnetic torque exerted on the particle. The first part, which involves the particle stress as a function of the particle magnetic moment, is determined from the Maxwell force moment on the particle in § 2 and appendix A. This calculation is restricted to a spherical particle, and is valid in the continuum limit.

The second part of the calculation is described in appendix A of Kumaran (2019). In the third part of the calculation in § 3, the angular velocity and the magnetic moment are determined from the torque balance condition for specified values of the fluid vorticity at the particle centre and the magnetic field. From this, the expression for the particle stress tensor is derived. The expression for the stress tensor contains three symmetric stress coefficients for the shear stress in the three perpendicular planes in the $(\hat{\boldsymbol{\omega}}, \hat{\boldsymbol{e}}_{\parallel}, \hat{\boldsymbol{e}}_{\perp})$ space, and two coefficients for the normal stress difference, in addition to the three antisymmetric stress coefficients calculated in Kumaran (2019). In the expression for the stress tensor, there are terms linear in the particle magnetic moment, due to the interaction of the moment with the external field, and a term that is a quadratic function of the magnetic moment. It is shown that the quadratic term is numerically much smaller than the terms that are linear in the magnetic moment. A simplified expression for the stress tensor is derived in the 'linear' approximation, where the quadratic terms in the stress tensor are neglected. In the linear approximation, the simplified expression for the stress contains only two stress coefficients.

The calculation of the particle stress from the magnetic moment and the calculation of the eddy current due to particle rotation are valid for a spherical particle or shell of any size with uniform electrical resistivity. The particle is considered to be a conducting continuum and the fluid is an insulating continuum. For both particle and fluid, the magnetic permeability is assumed to be that of vacuum. The torque balance condition assumes the limit of low Reynolds number, so that the sum of the hydrodynamic and magnetic torques is zero. It should be emphasised that the particles are not ferromagnetic, and they do not have a permanent dipole moment or magnetic polarisation. There is a particle dipole moment due to eddy currents only when a particle is rotating, and there is no dipole moment when the particle is stationary.

In appendix C, the particle stress in a suspension of charged particles in a magnetic field is determined. This calculation is simpler than that for a conducting particle, because an analytical solution can be obtained for the particle angular velocity and particle stress coefficients as a function of the particle charge, diameter, fluid vorticity and magnetic field. The magnetic dipole moment $\boldsymbol{M}$ due to a particle with radius R and charge Q rotating with angular velocity $\boldsymbol{\Omega}$ is $C_{\Omega}\boldsymbol{\Omega}R^2 Q$, where C_{Ω} is a dimensionless constant that depends on the distribution of charges in the particle. The torque balance equation (sum of hydrodynamic and magnetic torques is zero) can be solved analytically to obtain the particle angular velocity as a function of the fluid vorticity $\boldsymbol{\omega}$. The particle stress depends on two dimensionless parameters: the vorticity-independent parameter $\Sigma_{ch} = (C_{\Omega}Q\mu_0 H_0/8\pi\eta R)$ and the parameter $\beta_{ch} = (C_{\Omega}^2 Q^2 \mu_0 |\boldsymbol{\omega}|/(8\pi)^2 \eta R^2)$ which is the ratio of the vorticity and the charge relaxation time. In § 4.1, it is shown that the parameter Σ_{ch} is numerically small and β_{ch} is negligible in practical applications, and a simplified expression for the particle stress is obtained. The main conclusions are provided in § 4.

2. Particle stress

The magnetic field $\boldsymbol{H}$ around a spherical particle due to the magnetic moment $\boldsymbol{M}$ at the centre of the particle (Landau *et al.* 2014) is

$$\boldsymbol{H} = \boldsymbol{H}_0 + \frac{1}{4\pi}\left(\frac{3(\boldsymbol{x} - \boldsymbol{x}_c)(\boldsymbol{x} - \boldsymbol{x}_c)}{|\boldsymbol{x} - \boldsymbol{x}_c|^5} - \frac{\boldsymbol{I}}{|\boldsymbol{x} - \boldsymbol{x}_c|^3}\right) \cdot \boldsymbol{M}, \quad (2.1)$$

where $\boldsymbol{H}_0$ is the applied magnetic field, $\boldsymbol{x}$ is the position vector, $\boldsymbol{x}_c$ is the centre of the spherical particle, $\boldsymbol{I}$ is the isotropic tensor and $\boldsymbol{M}$ is the magnetic moment of the particle.

The Maxwell stress is given by

$$\boldsymbol{\sigma}^M = \mu_0(\boldsymbol{H}\boldsymbol{H} - \tfrac{1}{2}\boldsymbol{I}(\boldsymbol{H} \cdot \boldsymbol{H})), \tag{2.2}$$

where μ_0 is the magnetic permeability of free space. The particle stress $\boldsymbol{\sigma}^p$ due to the magnetic field is related to the symmetric force moment integrated over the particle surface (Batchelor 1970):

$$\boldsymbol{\sigma}^p = \frac{\phi}{(4\pi R^3/3)} \int_S \mathrm{d}S\,(\boldsymbol{x} - \boldsymbol{x}_c)\boldsymbol{n} \cdot \left[\boldsymbol{\sigma}^M - \mu_0 \left(\boldsymbol{H}_0\boldsymbol{H}_0 - \frac{1}{2}\boldsymbol{I}(\boldsymbol{H}_0 \cdot \boldsymbol{H}_0) \right) \right], \tag{2.3}$$

where S is the surface of the sphere, $\boldsymbol{n} = ((\boldsymbol{x} - \boldsymbol{x}_c)/|\boldsymbol{x} - \boldsymbol{x}_c|)$ is the outward unit normal to the sphere, R is the particle radius and ϕ is the volume fraction of the particles. It is important to note that the stresses $\boldsymbol{\sigma}^p$ and $\boldsymbol{\sigma}^M$ in (2.3) have been defined such that the first index of the tensor is the direction of the unit normal to the surface and the second index is the direction of the force. In (2.3), the background uniform stress $(\boldsymbol{H}_0\boldsymbol{H}_0 - \frac{1}{2}\boldsymbol{I}(\boldsymbol{H}_0 \cdot \boldsymbol{H}_0))$ has been subtracted to obtain the excess particle stress. The detailed calculation of the particle stress is provided in appendix A, and the final result for the particle stress is

$$\boldsymbol{\sigma}^p = \mu_0\phi \left[\frac{\boldsymbol{M}\boldsymbol{H}_0 + \boldsymbol{H}_0\boldsymbol{M}}{8\pi R^3} - \frac{\boldsymbol{M}\boldsymbol{M}}{80\pi^2 R^6} + \boldsymbol{I}\left(\frac{\boldsymbol{H}_0 \cdot \boldsymbol{M}}{4\pi R^3} + \frac{\boldsymbol{M} \cdot \boldsymbol{M}}{40\pi^2 R^6} \right) \right]$$
$$+ \frac{3\mu_0\phi(\boldsymbol{M}\boldsymbol{H}_0 - \boldsymbol{H}_0\boldsymbol{M})}{8\pi R^3}. \tag{2.4}$$

The stress can be separated into the symmetric traceless part, the antisymmetric part and the isotropic part, $\boldsymbol{\sigma}^p = \boldsymbol{\sigma}^p_e + \boldsymbol{\sigma}^p_a + \boldsymbol{\sigma}^p_i$:

$$\boldsymbol{\sigma}^p_e = \mu_0\phi \left[\frac{\boldsymbol{M}\boldsymbol{H}_0 + \boldsymbol{H}_0\boldsymbol{M} - \dfrac{2}{3}\boldsymbol{I}(\boldsymbol{H}_0 \cdot \boldsymbol{M})}{8\pi R^3} - \frac{\boldsymbol{M}\boldsymbol{M} - \dfrac{1}{3}\boldsymbol{I}(\boldsymbol{M} \cdot \boldsymbol{M})}{80\pi^2 R^6} \right], \tag{2.5}$$

$$\boldsymbol{\sigma}^p_a = \mu_0\phi \left[\frac{3(\boldsymbol{M}\boldsymbol{H}_0 - \boldsymbol{H}_0\boldsymbol{M})}{8\pi R^3} \right], \tag{2.6}$$

$$\boldsymbol{\sigma}^p_i = \mu_0\phi\boldsymbol{I} \left[\frac{\boldsymbol{H}_0 \cdot \boldsymbol{M}}{3\pi R^3} + \frac{\boldsymbol{M} \cdot \boldsymbol{M}}{48\pi^2 R^6} \right]. \tag{2.7}$$

The isotropic part of the stress tensor, (2.7), can be subsumed in the fluid pressure, and so it does not affect the flow. The antisymmetric part of the stress tensor, (2.6), is the same as that determined from the torque on a particle, (1.1), in Kumaran (2019).

3. Rheology

3.1. *Magnetic moment*

A brief summary of the solution procedure for the angular velocity of a conducting particle in a magnetic field is provided here, since the procedure is described in detail in Kumaran (2019). A conducting particle in a magnetic field $\boldsymbol{H}_0$ is considered, where the fluid vorticity at the particle centre in the absence of the particle is $\boldsymbol{\omega}$. The angular velocity is non-dimensionalised by one half of the fluid vorticity $\boldsymbol{\omega}$, $\boldsymbol{\Omega}^* = (\boldsymbol{\Omega}/(|\boldsymbol{\omega}|/2))$, so that the non-dimensional angular velocity is 1 in the absence of a torque on the particle. The torque

balance equations were solved in an orthogonal coordinate system shown in figure 1(*b*), where the three orthogonal coordinates are

$$\hat{\boldsymbol{\omega}} = \frac{\boldsymbol{\omega}}{|\boldsymbol{\omega}|}, \tag{3.1}$$

the unit vector along the vorticity direction,

$$\hat{\boldsymbol{e}}_{\parallel} = \frac{\hat{\boldsymbol{H}} - \hat{\boldsymbol{\omega}}(\hat{\boldsymbol{\omega}} \cdot \hat{\boldsymbol{H}})}{\sqrt{1 - (\hat{\boldsymbol{\omega}} \cdot \hat{\boldsymbol{H}})^2}}, \tag{3.2}$$

the unit vector perpendicular to $\hat{\boldsymbol{\omega}}$ in the $\hat{\boldsymbol{\omega}}$–$\hat{\boldsymbol{H}}$ plane, and

$$\hat{\boldsymbol{e}}_{\perp} = \frac{\hat{\boldsymbol{\omega}} \times \hat{\boldsymbol{H}}}{\sqrt{1 - (\hat{\boldsymbol{\omega}} \cdot \hat{\boldsymbol{H}})^2}}, \tag{3.3}$$

the unit vector perpendicular to the $\hat{\boldsymbol{\omega}}$–$\hat{\boldsymbol{H}}$ plane. The unit vector $\hat{\boldsymbol{\Omega}}$ (figure 1*a*) along the direction of the angular velocity is resolved into three components, $\hat{\Omega}_{\omega} = \hat{\boldsymbol{\Omega}} \cdot \hat{\boldsymbol{\omega}}$, $\hat{\Omega}_{\parallel} = \hat{\boldsymbol{\Omega}} \cdot \hat{\boldsymbol{e}}_{\parallel}$ and $\hat{\Omega}_{\perp} = \hat{\boldsymbol{\Omega}} \cdot \hat{\boldsymbol{e}}_{\perp}$. The projection of the unit angular velocity vector onto the direction of the magnetic field is

$$\hat{\Omega}_H = \hat{\Omega}_{\omega}(\hat{\boldsymbol{\omega}} \cdot \hat{\boldsymbol{H}}) + \hat{\Omega}_{\parallel}\sqrt{1 - (\hat{\boldsymbol{\omega}} \cdot \hat{\boldsymbol{H}})^2}. \tag{3.4}$$

There are two dimensionless parameters in the torque balance equations. The parameter $\Sigma = (\mu_0 H_0^2 / 4\pi\eta|\boldsymbol{\omega}|)$ is the ratio of the magnetic stress and the viscous stress, where η is the fluid viscosity. The parameter β is the product of the current relaxation time and the vorticity. For a uniform spherical particle, $\beta = \beta_p = (|\boldsymbol{\omega}|\mu_0 R^2 / 2\varrho)$, where R is the particle radius and ϱ is the electrical resistivity. For a thin conducting shell of outer radius R and thickness δR, with $\delta \ll 1$, the parameter $\beta = \beta_s = (|\boldsymbol{\omega}|\mu_0 R^2 \delta / 2\varrho)$. Since there is no magnetic torque along the direction of the magnetic field, the torque balance condition requires that the components of the angular velocity vector and one half of the vorticity vector along the direction of the magnetic field are equal. This condition can be written in terms of the dimensionless angular velocity Ω^* as

$$\hat{\boldsymbol{\omega}} \cdot \hat{\boldsymbol{H}} = \Omega^* \hat{\Omega}_H, \tag{3.5}$$

where $\Omega^* = |\boldsymbol{\Omega}^*|$.

The sum of the hydrodynamic torque, $8\pi\eta R^3((\boldsymbol{\omega}/2) - \boldsymbol{\Omega})$, and the magnetic torque, $\boldsymbol{M} \times (\mu_0\boldsymbol{H}_0)$, is set equal to zero in the limit of low Reynolds number to determine the particle angular velocity. The torque balance equations in the $\hat{\boldsymbol{\omega}}$, $\hat{\boldsymbol{e}}_{\parallel}$ and $\hat{\boldsymbol{e}}_{\perp}$ directions (Kumaran 2019) reduce to

$$\hat{\Omega}_{\omega} - \Omega^* - \Sigma(1 - \hat{\Omega}_H^2)M_I^*(\beta\Omega^*) = 0, \tag{3.6}$$

$$\hat{\boldsymbol{\omega}} \cdot \hat{\boldsymbol{H}} - \hat{\Omega}_{\omega}\hat{\Omega}_H + \Sigma\hat{\Omega}_H(1 - \hat{\Omega}_H^2)M_I^*(\beta\Omega^*) = 0, \tag{3.7}$$

$$\hat{\boldsymbol{\omega}} \cdot (\hat{\boldsymbol{\Omega}} \times \hat{\boldsymbol{H}}) - \Sigma\hat{\Omega}_H(1 - \hat{\Omega}_H^2)M_R^*(\beta\Omega^*) = 0. \tag{3.8}$$

Equation (3.8) is recast in terms of $\hat{e}_\perp$:

$$\hat{\Omega}_\perp \sqrt{1 - (\hat{\boldsymbol{\omega}} \cdot \hat{H})^2} + \Sigma \hat{\Omega}_H (1 - \hat{\Omega}_H^2) M_R^*(\beta \Omega^*) = 0, \qquad (3.9)$$

where $\hat{\Omega}_\perp = \boldsymbol{\Omega} \cdot \hat{e}_\perp$. The dimensionless functions M_R^* and M_I^* appearing in the expression for the particle magnetic moment calculated in Kumaran (2019) are provided in appendix B, and the asymptotic limits of these functions are listed in table 3. The function $M_R^*(\beta \Omega^*)$ is negative for positive $\beta \Omega^*$, its magnitude increases proportional to $(\beta \Omega^*)^2$ for $\beta \Omega^* \ll 1$ and the function tends to a constant value of $-\frac{1}{2}$ for $\beta \Omega^* \gg 1$. The function $M_I^*(\beta \Omega^*)$ is positive, its magnitude increases proportional to $\beta \Omega^*$ for $\beta \Omega^* \ll 1$ and decreases proportional to $(\beta_p \Omega^*)^{-1/2}$ for a uniform particle and proportional to $(\beta_s \Omega^*)^{-1}$ for a thin shell for $\beta \Omega^* \gg 1$.

The solution is obtained in the following sequence. Equation (3.5) is used to express Ω^* in terms of $(\hat{\boldsymbol{\omega}} \cdot \hat{H})$ and $\hat{\Omega}_H$, then $\hat{\Omega}_\omega$ is expressed as a function of $(\hat{\boldsymbol{\omega}} \cdot \hat{H})$ and $\hat{\Omega}_H$, using (3.6), $\hat{\Omega}_\parallel$ is expressed in terms of $(\hat{\boldsymbol{\omega}} \cdot \hat{H})$ and $\hat{\Omega}_H$ using (3.4), and $\hat{\Omega}_\perp$ is expressed in terms of $(\hat{\boldsymbol{\omega}} \cdot \hat{H})$ and $\hat{\Omega}_H$ using (3.9). Since $\hat{\boldsymbol{\Omega}}$ is a unit vector, the requirement that $\hat{\Omega}_\omega^2 + \hat{\Omega}_\parallel^2 + \hat{\Omega}_\perp^2 = 1$ provides an implicit relation for $\hat{\Omega}_H$ in terms of $\hat{\boldsymbol{\omega}} \cdot \hat{H}$, Σ and β. This equation is solved to determine $\hat{\Omega}_H$ (whose magnitude is not greater than 1) as a function of $(\hat{\boldsymbol{\omega}} \cdot \hat{H})$, Σ and β.

The transformation of the solutions upon change in sign of $\hat{\boldsymbol{\omega}} \cdot \hat{H}$ is as follows. From (3.5), it is evident that when the sign of $\hat{\boldsymbol{\omega}} \cdot \hat{H}$ is reversed, the sign of $\hat{\Omega}_H$ is also reversed because Ω^* is the magnitude of the angular velocity. When the sign of $\hat{\boldsymbol{\omega}} \cdot \hat{H}$ is reversed, (3.6) and (3.7) are unchanged if the sign of $\hat{\Omega}_\omega$ is unchanged, (3.4) is unchanged if the sign of $\hat{\Omega}_\parallel$ is reversed and (3.9) is unchanged if the sign of $\hat{\Omega}_\perp$ is reversed. Consequently, there is the transformation $\hat{\Omega}_H \to -\hat{\Omega}_H$, $\Omega^* \to \Omega^*$, $\hat{\Omega}_\omega \to \hat{\Omega}_\omega$, $\hat{\Omega}_\parallel \to -\hat{\Omega}_\parallel$ and $\hat{\Omega}_\perp \to -\hat{\Omega}_\perp$ upon the sign reversal $\hat{\boldsymbol{\omega}} \cdot \hat{H} \to -\hat{\boldsymbol{\omega}} \cdot \hat{H}$.

The particle angular velocity and the torque on the particle were determined as a function of $(\hat{\boldsymbol{\omega}} \cdot \hat{H})$, Σ and β in Kumaran (2019). The solutions for the angular velocity and torque are unique for small and moderate values of β, but there was the possibility of multiple (three) steady states for $\beta_p > 93$ for a uniform particle and for $\beta_s > 15.7$ for a thin shell when the magnetic field is perpendicular to the vorticity. The antisymmetric component of the stress tensor was determined, but the symmetric part is not accessible from the torque on a particle. In the present study, the symmetric part of the stress tensor is determined from the induced magnetic moment on the particle using (2.5).

The induced magnetic moment of the conducting particle is expressed as $\boldsymbol{M} = H_0 R^3 \boldsymbol{M}^*$, where $\boldsymbol{M}^*$ is the dimensionless magnetic moment:

$$\boldsymbol{M}^* = M_R^*(\beta \Omega^*)(\hat{H} - \hat{\Omega}_H \hat{\boldsymbol{\Omega}}) + M_I^*(\beta \Omega^*)(\hat{\boldsymbol{\Omega}} \times \hat{H}). \qquad (3.10)$$

It is useful to note here that $\boldsymbol{M}^* \cdot \boldsymbol{\Omega} = 0$, that is, the magnetic moment is necessarily perpendicular to the axis of rotation for a conducting particle. The magnetic moment is resolved in the three orthogonal directions $\hat{\boldsymbol{\omega}}$, $\hat{e}_\parallel$ and $\hat{e}_\perp$, in order to determine the particle stress. The dimensionless magnetic moment in the vorticity direction is

$$\begin{aligned} M_\omega^* &= M_R^*(\beta \Omega^*)(\hat{\boldsymbol{\omega}} \cdot \hat{H} - \hat{\Omega}_\omega \hat{\Omega}_H) + M_I^*(\beta \Omega^*)(\hat{\boldsymbol{\omega}} \cdot (\hat{\boldsymbol{\Omega}} \times \hat{H})) \\ &= 0. \end{aligned} \qquad (3.11)$$

Here, the torque balance (3.7) and (3.8) have been used to substitute for $(\hat{\boldsymbol{\omega}} \cdot \hat{\boldsymbol{H}} - \hat{\Omega}_\omega \hat{\Omega}_H)$ and $\hat{\boldsymbol{\omega}} \cdot (\hat{\boldsymbol{\Omega}} \times \hat{\boldsymbol{H}})$. Equation (3.11) is a significant result, which states that the component of the magnetic moment along the vorticity direction is zero . Since the component of the magnetic moment along the direction of the angular velocity is also zero, (3.11) uniquely specifies the direction of the magnetic moment perpendicular to the plane containing the particle angular velocity and the fluid vorticity for the general case where the angular velocity and vorticity are not parallel.

The component of the magnetic moment perpendicular to $\hat{\boldsymbol{\omega}}$ in the $\hat{\boldsymbol{\omega}}$–$\hat{\boldsymbol{H}}$ plane is

$$M_\parallel^* = \frac{M_R^*(\beta\Omega^*)(1 - \hat{\Omega}_H^2)}{\sqrt{1 - (\hat{\boldsymbol{\omega}} \cdot \hat{\boldsymbol{H}})^2}}. \tag{3.12}$$

The component of the magnetic moment perpendicular to the $\hat{\boldsymbol{\omega}}$–$\hat{\boldsymbol{H}}$ plane is

$$M_\perp^* = \frac{\Sigma(1 - \hat{\Omega}_H^2)(M_R^*(\beta\Omega^*)^2\hat{\Omega}_H^2 + M_I^*(\beta\Omega^*)^2)}{\sqrt{1 - (\hat{\boldsymbol{\omega}} \cdot \hat{\boldsymbol{H}})^2}} + \frac{M_I^*(\beta\Omega^*)(1 - \hat{\Omega}_H^2)(\hat{\boldsymbol{\omega}} \cdot \hat{\boldsymbol{H}})}{\hat{\Omega}_H\sqrt{1 - (\hat{\boldsymbol{\omega}} \cdot \hat{\boldsymbol{H}})^2}}. \tag{3.13}$$

For the special case where the vorticity and magnetic field are perpendicular, the particle angular velocity is aligned along the vorticity direction, $\hat{\boldsymbol{\omega}} \cdot \hat{\boldsymbol{H}} = 0$, $\hat{\Omega}_H = 0$ and $\hat{\Omega}_\omega = 1$. The magnetic moments are

$$M_\parallel^* = M_R^*(\beta\Omega^*), \tag{3.14}$$
$$M_\perp^* = M_I^*(\beta\Omega^*). \tag{3.15}$$

In deriving (3.15), (3.5) has been used to express $\hat{\Omega}_H$ in terms of Ω^* and (3.6) has been used to substitute for $\Omega^* = 1 - \Sigma M_I^*(\beta\Omega^*)$.

3.2. *Particle stress*

The magnetic moments are substituted into (2.5) in order to determine the symmetric traceless part of the stress tensor. The stress is expressed in the coordinate system $(\hat{\boldsymbol{\omega}}, \hat{\boldsymbol{e}}_\parallel, \hat{\boldsymbol{e}}_\perp)$:

$$\begin{aligned}\boldsymbol{\sigma}^p = |\boldsymbol{\omega}|[&\eta_s^{(1)}(\hat{\boldsymbol{e}}_\parallel\hat{\boldsymbol{e}}_\perp + \hat{\boldsymbol{e}}_\perp\hat{\boldsymbol{e}}_\parallel) + \eta_s^{(2)}(\hat{\boldsymbol{e}}_\perp\hat{\boldsymbol{\omega}} + \hat{\boldsymbol{\omega}}\hat{\boldsymbol{e}}_\perp) + \eta_s^{(3)}(\hat{\boldsymbol{e}}_\parallel\hat{\boldsymbol{\omega}} + \hat{\boldsymbol{\omega}}\hat{\boldsymbol{e}}_\parallel) \\ &+ \eta_n^{(1)}(\hat{\boldsymbol{e}}_\parallel\hat{\boldsymbol{e}}_\parallel - \hat{\boldsymbol{e}}_\perp\hat{\boldsymbol{e}}_\perp) + \eta_n^{(2)}(\hat{\boldsymbol{e}}_\perp\hat{\boldsymbol{e}}_\perp - \hat{\boldsymbol{\omega}}\hat{\boldsymbol{\omega}}) \\ &+ \eta_a^{(1)}(\hat{\boldsymbol{e}}_\parallel\hat{\boldsymbol{e}}_\perp - \hat{\boldsymbol{e}}_\perp\hat{\boldsymbol{e}}_\parallel) + \eta_a^{(2)}(\hat{\boldsymbol{e}}_\perp\hat{\boldsymbol{\omega}} - \hat{\boldsymbol{\omega}}\hat{\boldsymbol{e}}_\perp) + \eta_a^{(3)}(\hat{\boldsymbol{\omega}}\hat{\boldsymbol{e}}_\parallel - \hat{\boldsymbol{e}}_\parallel\hat{\boldsymbol{\omega}})], \end{aligned} \tag{3.16}$$

where the symmetric, normal and antisymmetric stress coefficients are

$$\eta_s^{(1)} = \eta\phi\Sigma\left[\frac{\sqrt{1 - (\hat{\boldsymbol{\omega}} \cdot \hat{\boldsymbol{H}})^2}M_\perp^*}{2} - \frac{M_\parallel^*M_\perp^*}{20\pi}\right], \tag{3.17}$$

$$\eta_s^{(2)} = \eta\phi\Sigma\left[\frac{(\hat{\boldsymbol{\omega}} \cdot \hat{\boldsymbol{H}})M_\perp^*}{2}\right], \tag{3.18}$$

$$\eta_s^{(3)} = \eta\phi\,\Sigma\left[\frac{(\hat{\boldsymbol{\omega}}\cdot\hat{\boldsymbol{H}})M_\parallel^*}{2}\right], \tag{3.19}$$

$$\eta_n^{(1)} = \eta\phi\,\Sigma\left[\sqrt{1-(\hat{\boldsymbol{\omega}}\cdot\hat{\boldsymbol{H}})^2}M_\parallel^* - \frac{M_\parallel^{*2}-M_\perp^{*2}}{20\pi}\right], \tag{3.20}$$

$$\eta_n^{(2)} = -\eta\phi\,\Sigma\left[\frac{M_\perp^{*2}}{20\pi}\right], \tag{3.21}$$

$$\eta_a^{(1)} = -\frac{3\eta\phi\,\Sigma\sqrt{1-(\hat{\boldsymbol{\omega}}\cdot\hat{\boldsymbol{H}})^2}M_\perp^*}{2}, \tag{3.22}$$

$$\eta_a^{(2)} = \frac{3\eta\phi\,\Sigma\,(\hat{\boldsymbol{\omega}}\cdot\hat{\boldsymbol{H}})M_\perp^*}{2}, \tag{3.23}$$

$$\eta_a^{(3)} = -\frac{3\eta\phi\,\Sigma\,(\hat{\boldsymbol{\omega}}\cdot\hat{\boldsymbol{H}})M_\parallel^*}{2}. \tag{3.24}$$

The antisymmetric stress coefficients, (3.22)–(3.24), have been calculated from the torque on a particle in Kumaran (2019), and the dependence of these on the parameters Σ and β has been discussed in detail. It has been verified that the results obtained from (3.22)–(3.24) are in quantitative agreement with those in Kumaran (2019).

Asymptotic expressions can be obtained for the symmetric and normal stress coefficients in the limit $\Sigma \ll 1$ using a regular perturbation expansion in the parameter Σ, and in the limit $\Sigma \gg 1$ using a regular perturbation expansion in the parameter Σ^{-1}. These expressions are shown in table 1, along with the expansions for the moments $M_\parallel^*$ and $M_\perp^*$. In the limit $\Sigma \ll 1$, the magnetic field has a small effect on the particle rotation, and the difference between the particle angular velocity and the fluid vorticity is $O(\Sigma)$. The scaled angular velocity Ω^* is equal to 1 in the leading approximation, and the magnetic moments and antisymmetric stress coefficients depend on the functions $M_R(\beta)$ and $M_I(\beta)$. In the limit $\Sigma \gg 1$, the particle angular velocity is aligned close to the magnetic field, and the dot product $\hat{\Omega}_H$ differs from 1 by $O(\Sigma^{-1})$. For $\hat{\Omega}_H \cong 1$, it can be inferred from (3.5) that $\Omega^* \sim \hat{\boldsymbol{\omega}}\cdot\hat{\boldsymbol{H}}$, and therefore the scaled magnetic moments and stress coefficients depend on $M_R(\beta\hat{\boldsymbol{\omega}}\cdot\hat{\boldsymbol{H}})$ and $M_I(\beta\hat{\boldsymbol{\omega}}\cdot\hat{\boldsymbol{H}})$. The asymptotic expressions for the antisymmetric stress coefficients are provided in Kumaran (2019).

Table 1 shows that the stress coefficients have the same dependence on $(\hat{\boldsymbol{\omega}}\cdot\hat{\boldsymbol{H}})$ in the limits $\Sigma \ll 1$ and $\Sigma \gg 1$, and therefore it is possible to define scaled stress coefficients which are independent of $(\hat{\boldsymbol{\omega}}\cdot\hat{\boldsymbol{H}})$ in the limits of low and high Σ:

$$\eta_s^{(1)} = \eta\phi(1-(\hat{\boldsymbol{\omega}}\cdot\hat{\boldsymbol{H}})^2)\bar{\eta}_s^{(1)}, \tag{3.25}$$

$$\eta_s^{(2)} = \eta\phi(\hat{\boldsymbol{\omega}}\cdot\hat{\boldsymbol{H}})\sqrt{1-(\hat{\boldsymbol{\omega}}\cdot\hat{\boldsymbol{H}})^2}\bar{\eta}_s^{(2)}, \tag{3.26}$$

$$\eta_s^{(3)} = \eta\phi(\hat{\boldsymbol{\omega}}\cdot\hat{\boldsymbol{H}})\sqrt{1-(\hat{\boldsymbol{\omega}}\cdot\hat{\boldsymbol{H}})^2}\bar{\eta}_s^{(3)}, \tag{3.27}$$

$$\eta_n^{(1)} = \eta\phi(1-(\hat{\boldsymbol{\omega}}\cdot\hat{\boldsymbol{H}})^2)\bar{\eta}_n^{(1)}, \tag{3.28}$$

$$\eta_n^{(2)} = \eta\phi(1-(\hat{\boldsymbol{\omega}}\cdot\hat{\boldsymbol{H}})^2)\bar{\eta}_n^{(2)}. \tag{3.29}$$

	$\Sigma \ll 1$	$\Sigma \gg 1$
$M_\parallel^*$	$\sqrt{1-(\hat{\boldsymbol{\omega}}\cdot\hat{\boldsymbol{H}})^2}\,M_R^*(\beta)$	$\dfrac{\sqrt{1-(\hat{\boldsymbol{\omega}}\cdot\hat{\boldsymbol{H}})^2}\,M_R^*(\beta\hat{\boldsymbol{\omega}}\cdot\hat{\boldsymbol{H}})}{\Sigma(M_R^*(\beta\hat{\boldsymbol{\omega}}\cdot\hat{\boldsymbol{H}})^2+M_I^*(\beta\hat{\boldsymbol{\omega}}\cdot\hat{\boldsymbol{H}})^2)}$
$M_\perp^*$	$\sqrt{1-(\hat{\boldsymbol{\omega}}\cdot\hat{\boldsymbol{H}})^2}\,M_I^*(\beta)$	$\sqrt{1-(\hat{\boldsymbol{\omega}}\cdot\hat{\boldsymbol{H}})^2}+\dfrac{(\hat{\boldsymbol{\omega}}\cdot\hat{\boldsymbol{H}})\sqrt{1-(\hat{\boldsymbol{\omega}}\cdot\hat{\boldsymbol{H}})^2}\,M_I^*(\beta\hat{\boldsymbol{\omega}}\cdot\hat{\boldsymbol{H}})}{\Sigma(M_R^*(\beta\hat{\boldsymbol{\omega}}\cdot\hat{\boldsymbol{H}})^2+M_I^*(\beta\hat{\boldsymbol{\omega}}\cdot\hat{\boldsymbol{H}})^2)}$
$(\eta_s^{(1)}/\eta\phi)$	$\Sigma(1-(\hat{\boldsymbol{\omega}}\cdot\hat{\boldsymbol{H}})^2)$ $\times\left[\dfrac{M_I^*(\beta)}{2}-\dfrac{M_R^*(\beta)M_I^*(\beta)}{20\pi}\right]$	$(1-(\hat{\boldsymbol{\omega}}\cdot\hat{\boldsymbol{H}})^2)$ $\times\left[\dfrac{1}{2}+\dfrac{\hat{\boldsymbol{\omega}}\cdot\hat{\boldsymbol{H}}M_I^*(\beta\hat{\boldsymbol{\omega}}\cdot\hat{\boldsymbol{H}})}{2\Sigma(M_R^*(\beta\hat{\boldsymbol{\omega}}\cdot\hat{\boldsymbol{H}})^2+M_I^*(\beta\hat{\boldsymbol{\omega}}\cdot\hat{\boldsymbol{H}})^2)}\right]$
$(\eta_s^{(2)}/\eta\phi)$	$\dfrac{\Sigma(\hat{\boldsymbol{\omega}}\cdot\hat{\boldsymbol{H}})\sqrt{1-(\hat{\boldsymbol{\omega}}\cdot\hat{\boldsymbol{H}})^2}\,M_I^*(\beta)}{2}$	$\hat{\boldsymbol{\omega}}\cdot\hat{\boldsymbol{H}}\sqrt{1-(\hat{\boldsymbol{\omega}}\cdot\hat{\boldsymbol{H}})^2}$ $\times\left[\dfrac{1}{2}+\dfrac{\hat{\boldsymbol{\omega}}\cdot\hat{\boldsymbol{H}}M_I^*(\beta\hat{\boldsymbol{\omega}}\cdot\hat{\boldsymbol{H}})}{2\Sigma(M_R^*(\beta\hat{\boldsymbol{\omega}}\cdot\hat{\boldsymbol{H}})^2+M_I^*(\beta\hat{\boldsymbol{\omega}}\cdot\hat{\boldsymbol{H}})^2)}\right]$
$(\eta_s^{(3)}/\eta\phi)$	$\dfrac{\Sigma(\hat{\boldsymbol{\omega}}\cdot\hat{\boldsymbol{H}})\sqrt{1-(\hat{\boldsymbol{\omega}}\cdot\hat{\boldsymbol{H}})^2}\,M_R^*(\beta)}{2}$	$(\hat{\boldsymbol{\omega}}\cdot\hat{\boldsymbol{H}})\sqrt{1-(\hat{\boldsymbol{\omega}}\cdot\hat{\boldsymbol{H}})^2}$ $\times\left[\dfrac{M_R^*(\beta\hat{\boldsymbol{\omega}}\cdot\hat{\boldsymbol{H}})}{2\Sigma(M_R^*(\beta\hat{\boldsymbol{\omega}}\cdot\hat{\boldsymbol{H}})^2+M_I^*(\beta\hat{\boldsymbol{\omega}}\cdot\hat{\boldsymbol{H}})^2)}\right]$
$(\eta_n^{(1)}/\eta\phi)$	$\Sigma(1-(\hat{\boldsymbol{\omega}}\cdot\hat{\boldsymbol{H}})^2)$ $\times\left[M_R^*(\beta)+\dfrac{(M_I^*(\beta)^2-M_R^*(\beta)^2)}{20\pi}\right]$	$(1-(\hat{\boldsymbol{\omega}}\cdot\hat{\boldsymbol{H}})^2)$ $\times\left[\dfrac{1}{20\pi\Sigma}+\dfrac{M_R^*(\beta\hat{\boldsymbol{\omega}}\cdot\hat{\boldsymbol{H}})}{\Sigma(M_R^*(\beta\hat{\boldsymbol{\omega}}\cdot\hat{\boldsymbol{H}})^2+M_I^*(\beta\hat{\boldsymbol{\omega}}\cdot\hat{\boldsymbol{H}})^2)}\right]$
$(\eta_n^{(2)}/\eta\phi)$	$-\dfrac{\Sigma(1-(\hat{\boldsymbol{\omega}}\cdot\hat{\boldsymbol{H}})^2)M_I^*(\beta)^2}{20\pi}$	$-\left[\dfrac{1-(\hat{\boldsymbol{\omega}}\cdot\hat{\boldsymbol{H}})^2}{20\pi\Sigma}\right]$

TABLE 1. The $\Sigma \ll 1$ and $\Sigma \gg 1$ limits for the scaled magnetic moments $M_\parallel^*$ (equation (3.12)) and $M_\perp^*$ (equation (3.13)), and the viscometric coefficients $\eta_s^{(1)}$–$\eta_s^{(2)}$ and $\eta_n^{(1)}$–$\eta_n^{(2)}$ (equations (3.17)–(3.21)). The functions M_R^* and M_I^* are defined in appendix B for a uniform particle and a thin shell.

The functions $\bar{\eta}_s^{(1)}$–$\bar{\eta}_n^{(2)}$ are shown as a function of Σ for for different values of $(\hat{\boldsymbol{\omega}}\cdot\hat{\boldsymbol{H}})$ in figure 2 for a uniform particle and in figure 3 for a thin shell. The following results can be inferred from these figures.

(a) The first symmetric stress coefficient $\eta_s^{(1)}$ is positive and the first normal stress coefficient $\eta_n^{(1)}$ is negative. The sign of $\eta_s^{(2)}$ is the same as that of $\hat{\boldsymbol{\omega}}\cdot\hat{\boldsymbol{H}}$, while that of $\eta_s^{(3)}$ is the negative of that of $\hat{\boldsymbol{\omega}}\cdot\hat{\boldsymbol{H}}$. The second normal stress coefficient $\eta_n^{(2)}$ is always negative. This follows from (3.12) and (3.13), where it was shown that $M_\parallel$ and $M_\perp$ are negative and positive, respectively. Equations (3.22)–(3.24) indicate that the first antisymmetric stress coefficient is negative and the second and third antisymmetric stress coefficients have the same sign as $\hat{\boldsymbol{\omega}}\cdot\hat{\boldsymbol{H}}$. This is consistent with the results in Kumaran (2019).

(b) Excellent data collapse is observed for different values of $(\hat{\boldsymbol{\omega}}\cdot\hat{\boldsymbol{H}})$ for $\beta_p \leq 10$ for a uniform particle and $\beta_s \leq 3$ for a thin shell, indicating that the scalings (3.25)–(3.29) provide results that are independent of $\hat{\boldsymbol{\omega}}\cdot\hat{\boldsymbol{H}}$ for all the stress coefficients. In the regime
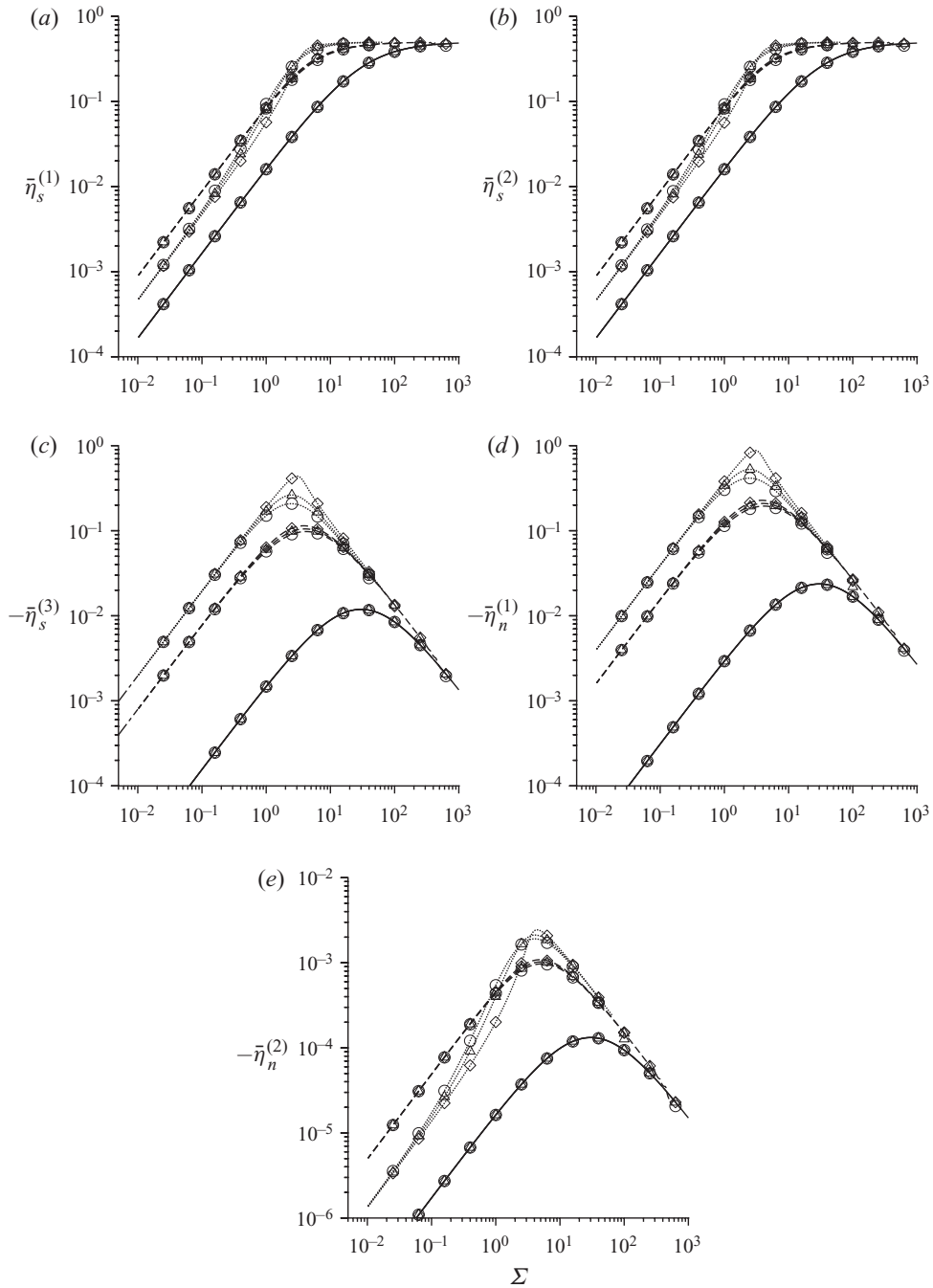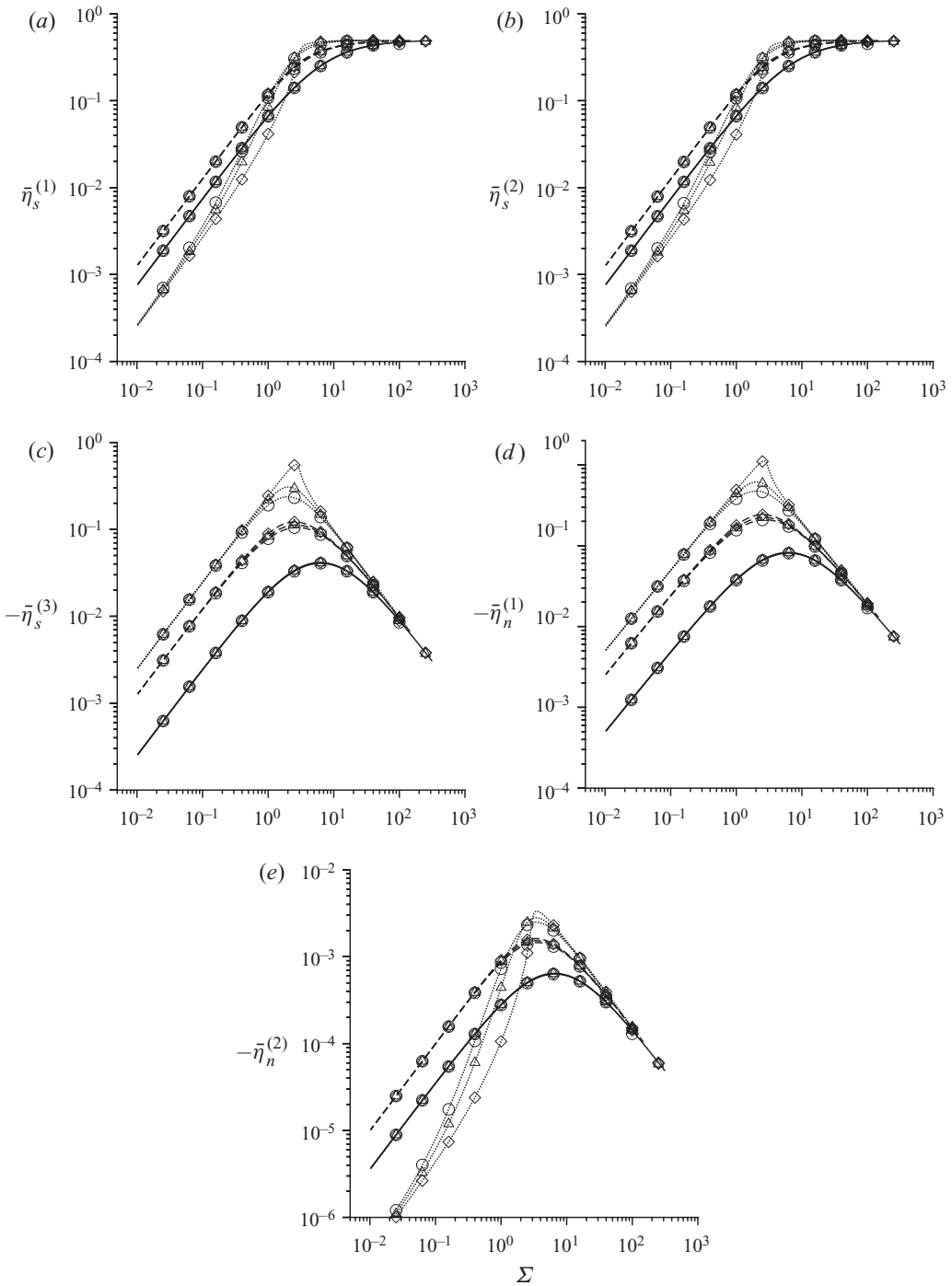
FIGURE 2. The scaled symmetric and normal viscosity coefficients $\bar{\eta}_s^{(1)}$ (a), $\bar{\eta}_s^{(2)}$ (b), $-\bar{\eta}_s^{(3)}$ (c), $\bar{\eta}_n^{(1)}$ (d) and $-\bar{\eta}_n^{(2)}$ (e) as a function of Σ for a uniform particle with $\beta_p = 1$ (solid lines), $\beta_p = 10$ (dashed lines) and $\beta_p = 100$ (dotted lines) and for $\hat{\boldsymbol{\omega}} \cdot \hat{\boldsymbol{H}} = 0.95$ (○), $\hat{\boldsymbol{\omega}} \cdot \hat{\boldsymbol{H}} = (1/\sqrt{2})$ (△) and $\hat{\boldsymbol{\omega}} \cdot \hat{\boldsymbol{H}} = (1/3)$ (◇).

FIGURE 3. The scaled symmetric and normal viscosity coefficients $\bar{\eta}_s^{(1)}$ (*a*), $\bar{\eta}_s^{(2)}$ (*b*), $-\bar{\eta}_s^{(3)}$ (*c*), $\bar{\eta}_n^{(1)}$ (*d*) and $-\bar{\eta}_n^{(2)}$ (*e*) as a function of Σ for a thin shell with $\beta_s = 1$ (solid lines), $\beta_s = 3$ (dashed lines) and $\beta_s = 30$ (dotted lines) and for $\hat{\boldsymbol{\omega}} \cdot \hat{\boldsymbol{H}} = 0.95$ (○), $\hat{\boldsymbol{\omega}} \cdot \hat{\boldsymbol{H}} = (1/\sqrt{2})$ (△) and $\hat{\boldsymbol{\omega}} \cdot \hat{\boldsymbol{H}} = (1/3)$ (◇).

$\beta_p > 10$ for a spherical particle and $\beta_s > 3$ for a thin shell, the results for different $\hat{\boldsymbol{\omega}} \cdot \hat{\boldsymbol{H}}$ do not coincide for Σ in the range 1–10, but there is good collapse of the date outside of this range.

(*c*) All the stress coefficients increase proportional to Σ for $\Sigma \ll 1$. For $\Sigma \gg 1$, the first and second symmetric stress coefficients tend to 0.5 and -0.5, respectively, and the magnitudes of the third symmetric stress coefficient and the first normal stress coefficient decrease proportional to Σ^{-1}. These asymptotic trends are independent of the parameter β, and are consistent with the analytical results in table 1. In fact, the expressions in table 1 are in quantitative agreement with the $\Sigma \ll 1$ and $\Sigma \gg 1$ asymptotic expressions; the comparison is not shown in figures 2 and 3 to enhance clarity.

(*d*) The magnitude of the second normal stress coefficient is $O(10^{-2})$ smaller than the other coefficients, due to the numerical factor of $(20\pi)^{-1}$ in (3.21).

(*e*) The magnitudes of $\bar{\eta}_s^{(1)}$ and $\bar{\eta}_s^{(2)}$ are nearly equal, indicating that the numerical difference due to the second term in the square brackets on the right-hand side of (3.17) is insignificant. Similarly, the magnitudes of $2\bar{\eta}_s^{(3)}$ and $\bar{\eta}_n^{(1)}$ are almost equal, indicating that the second term in the square brackets in (3.20) is much smaller than the other terms.

3.3. *Linear approximation*

In the linear approximation, where only terms linear in $M_\parallel^*$ and $M_\perp^*$ are retained in (3.17)–(3.24), the second normal stress coefficient $\eta_n^{(2)}$ is zero, and the seven stress coefficients, (3.17)–(3.23), can be related to two positive functions, $\bar{\eta}'(\beta, \Sigma)$ and $\bar{\eta}''(\beta, \Sigma)$:

$$\bar{\eta}'(\beta, \Sigma, \hat{\boldsymbol{\omega}} \cdot \hat{\boldsymbol{H}}) = 2\bar{\eta}_s^{(1)} = 2\bar{\eta}_s^{(2)} = -\tfrac{2}{3}\bar{\eta}_a^{(1)} = \tfrac{2}{3}\bar{\eta}_a^{(2)} = (\Sigma M_\perp^* / \sqrt{1 - (\hat{\boldsymbol{\omega}} \cdot \hat{\boldsymbol{H}})^2}), \quad (3.30)$$

$$\beta\bar{\eta}''(\beta, \Sigma, \hat{\boldsymbol{\omega}} \cdot \hat{\boldsymbol{H}}) = -2\bar{\eta}_s^{(3)} = -\bar{\eta}_n^{(1)} = \tfrac{2}{3}\bar{\eta}_a^{(3)} = -(\Sigma M_\parallel^* / \sqrt{1 - (\hat{\boldsymbol{\omega}} \cdot \hat{\boldsymbol{H}})^2}), \quad (3.31)$$

where the definitions of the scaled antisymmetric stress coefficients, calculated in Kumaran (2019), are

$$\eta_a^{(1)} = \eta\phi(1 - (\hat{\boldsymbol{\omega}} \cdot \hat{\boldsymbol{H}})^2)\bar{\eta}_a^{(1)}, \quad (3.32)$$

$$\eta_a^{(2)} = \eta\phi(\hat{\boldsymbol{\omega}} \cdot \hat{\boldsymbol{H}})\sqrt{1 - (\hat{\boldsymbol{\omega}} \cdot \hat{\boldsymbol{H}})^2}\bar{\eta}_a^{(2)}, \quad (3.33)$$

$$\eta_a^{(3)} = \eta\phi(\hat{\boldsymbol{\omega}} \cdot \hat{\boldsymbol{H}})\sqrt{1 - (\hat{\boldsymbol{\omega}} \cdot \hat{\boldsymbol{H}})^2}\bar{\eta}_a^{(3)}. \quad (3.34)$$

Using the above approximations, the constitutive relation for the stress tensor is

$$\begin{aligned}
\boldsymbol{\sigma}^p = |\boldsymbol{\omega}|\eta\phi\{&\bar{\eta}'(\beta, \Sigma, \hat{\boldsymbol{\omega}} \cdot \hat{\boldsymbol{H}})[(1 - (\hat{\boldsymbol{\omega}} \cdot \hat{\boldsymbol{H}})^2)(2\hat{\boldsymbol{e}}_\perp\hat{\boldsymbol{e}}_\parallel - \hat{\boldsymbol{e}}_\parallel\hat{\boldsymbol{e}}_\perp) \\
&+ (\hat{\boldsymbol{\omega}} \cdot \hat{\boldsymbol{H}})\sqrt{1 - (\hat{\boldsymbol{\omega}} \cdot \hat{\boldsymbol{H}})^2}(2\hat{\boldsymbol{e}}_\perp\hat{\boldsymbol{\omega}} - \hat{\boldsymbol{\omega}}\hat{\boldsymbol{e}}_\perp)] \\
&+ \beta\bar{\eta}''(\beta, \Sigma, \hat{\boldsymbol{\omega}} \cdot \hat{\boldsymbol{H}})[(\hat{\boldsymbol{\omega}} \cdot \hat{\boldsymbol{H}})\sqrt{1 - (\hat{\boldsymbol{\omega}} \cdot \hat{\boldsymbol{H}})^2}(\hat{\boldsymbol{\omega}}\hat{\boldsymbol{e}}_\parallel - 2\hat{\boldsymbol{e}}_\parallel\hat{\boldsymbol{\omega}}) \\
&- (1 - (\hat{\boldsymbol{\omega}} \cdot \hat{\boldsymbol{H}})^2)(\hat{\boldsymbol{e}}_\parallel\hat{\boldsymbol{e}}_\parallel - \hat{\boldsymbol{e}}_\perp\hat{\boldsymbol{e}}_\perp)]\}. \quad (3.35)
\end{aligned}$$

The Σ and β dependences of $\bar{\eta}'$ and $\bar{\eta}''$ in the limits of large and small β are summarised in table 2 for a uniform particle and a thin shell; these are derived using the asymptotic expressions for M_R^* and M_I^* in table 3. The asymptotic expressions are compared with the

	Spherical particle				Thin shell			
	$\beta_p \ll 1$		$\beta_p \gg 1$		$\beta_s \ll 1$		$\beta_s \gg 1$	
	$\bar{\eta}'$	$\bar{\eta}''$	$\bar{\eta}'$	$\bar{\eta}''$	$\bar{\eta}'$	$\bar{\eta}''$	$\bar{\eta}'$	$\bar{\eta}''$
$\Sigma \ll 1$	$(\beta_p \Sigma/30)$	$(\beta_p \Sigma/315)$	$\boxed{(3\Sigma/2\sqrt{2\beta_p})}$	$\boxed{(\Sigma/2\beta_p)}$	$(\beta_s \Sigma/6)$	$(\beta_s \Sigma/18)$	$\boxed{(3\Sigma/2\beta_s)}$	$\boxed{(\Sigma/2\beta_s)}$
Cross-over	$\beta_p \Sigma = 30$	$\beta_p \Sigma = 31.5$	$\Sigma = 0.94\sqrt{\beta_p}$	$\Sigma = 2$	$\beta_s \Sigma = 6$	$\beta_s \Sigma = 6$	$\Sigma = 0.67\beta_s$	$\Sigma = 2$
$\Sigma \gg 1$	1	$(20/7\beta_p \Sigma)$	1	$(2/\beta_p \Sigma)$	1	$(2/\beta_s \Sigma)$	1	$(2/\beta_s \Sigma)$

TABLE 2. The functions $\bar{\eta}'$ and $\bar{\eta}''$ (equation (3.35)) in the limits of small and large β and small and large Σ for a uniform particle and a thin shell.
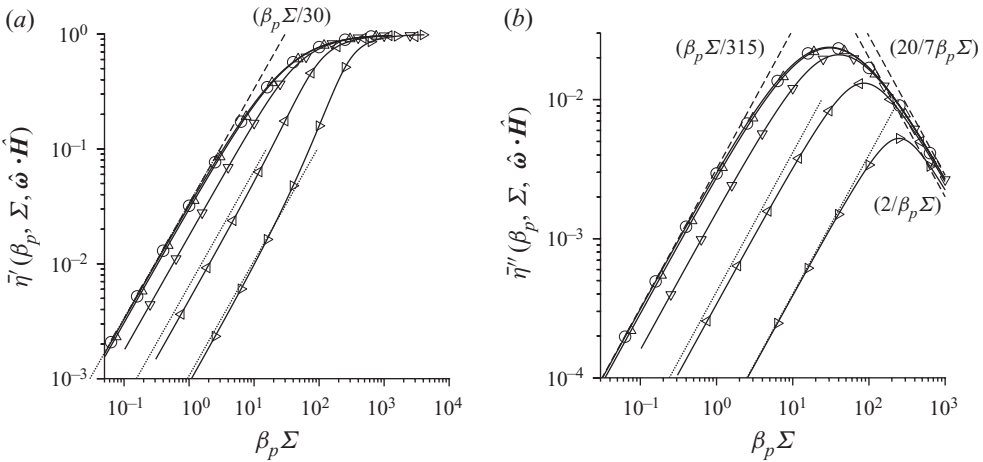
FIGURE 4. The functions $\bar{\eta}'(\beta_p, \Sigma, \hat{\boldsymbol{\omega}} \cdot \hat{\boldsymbol{H}})$ (*a*) and $\bar{\eta}''(\beta_p, \Sigma, \hat{\boldsymbol{\omega}} \cdot \hat{\boldsymbol{H}})$ (*b*) for a uniform particle for $\hat{\boldsymbol{\omega}} \cdot \hat{\boldsymbol{H}} = (1/\sqrt{2})$ and $\beta_p = 1$ (○), $\beta_p = 3$ (△), $\beta_p = 10$ (▽), $\beta_p = 30$ (◁) and $\beta_p = 100$ (▷). The dashed lines, from left to right, are the $\Sigma \ll 1$ and $\beta_p \gg 1$ asymptotic expressions in table 2 for $\beta_p = 30$ and 100, respectively.

actual numerical values in figure 4 for a uniform particle and in figure 5 for a thin shell. In all of the limits shown in table 2, the functions $\bar{\eta}'$ and $\bar{\eta}''$ are independent of $\hat{\boldsymbol{\omega}} \cdot \hat{\boldsymbol{H}}$, the angle between the vorticity and the magnetic field. In nearly all of the limits, $\bar{\eta}'$ and $\bar{\eta}''$ are functions only of the product $\beta \Sigma$; the only exceptions are the limits $\beta \gg 1$ and $\Sigma \ll 1$, shown by the boxed expressions in table 2. The intersection of the $\Sigma \ll 1$ and $\Sigma \gg 1$ asymptotes is also shown in table 2. For $\beta \ll 1$, the cross-over occurs at $\beta_p \Sigma \sim 30$ for a uniform particle and at $\beta_s \Sigma \sim 6$ for a thin shell. For $\beta \gg 1$, the location of the cross-over is $\Sigma = 2$ for the function $\bar{\eta}''$ for a uniform particle and a thin shell, but is dependent on β for the function $\bar{\eta}'$. From figures 2 and 3, it can further be inferred that the functions $\bar{\eta}'$ and $\bar{\eta}''$ are independent of $\hat{\boldsymbol{\omega}} \cdot \hat{\boldsymbol{H}}$, and they depend only on the product $\beta \Sigma$ for $\beta_p \lesssim 3$ for a uniform particle and $\beta_s \lesssim 1$ for a thin shell. In the limit $\beta \gg 1$ and $\Sigma \ll 1$, the numerical results are in agreement with the asymptotic predictions in table 2 only for $\beta_p \gtrsim 30$ for a uniform particle and $\beta_s \gtrsim 10$ for a thin shell.

The dependence of $\bar{\eta}'$ and $\bar{\eta}''$ only on the product $\beta \Sigma$ is significant, because this is a vorticity-independent parameter, which is $\beta_p \Sigma = (\mu_0^2 H_0^2 R^2/8\pi\eta\varrho)$ for a uniform particle
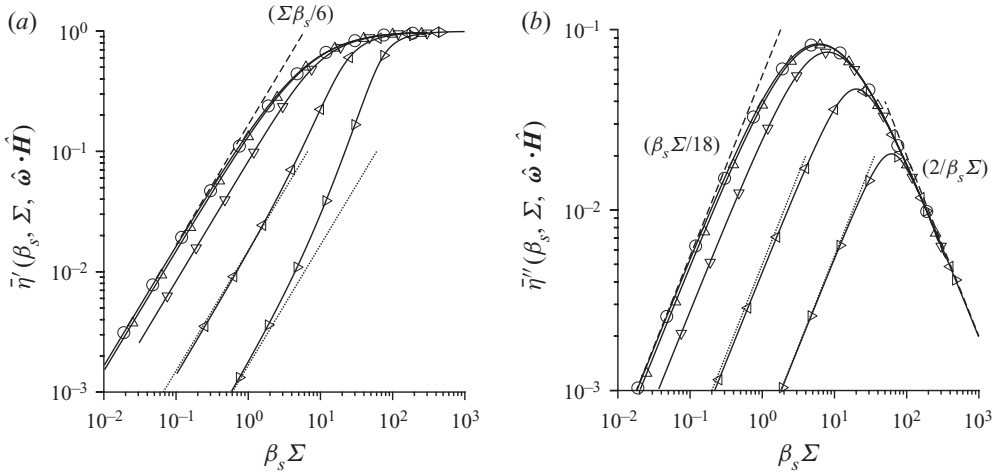
FIGURE 5. The functions $\bar{\eta}'(\beta_s, \Sigma, \hat{\boldsymbol{\omega}} \cdot \hat{\boldsymbol{H}})$ (a) and $\bar{\eta}''(\beta, \Sigma, \hat{\boldsymbol{\omega}} \cdot \hat{\boldsymbol{H}})$ (b) for a uniform particle for $\hat{\boldsymbol{\omega}} \cdot \hat{\boldsymbol{H}} = (1/\sqrt{2})$ and $\beta_s = 0.3$ (○), $\beta_s = 1$ (△), $\beta_s = 3$ (▽), $\beta_s = 10$ (◁) and $\beta_s = 30$ (▷). The dashed lines, from left to right, are the $\Sigma \ll 1$ and $\beta_s \gg 1$ asymptotic expressions in table 2 for $\beta_s = 10$ and 30, respectively.

and $\beta_s \Sigma = (\mu_0^2 H_0^2 R^2 \delta / 8\pi\eta\varrho)$. Therefore, the functions $\bar{\eta}'$ and $\bar{\eta}''$ depend only on material parameters and the magnetic field in most of the limits shown in table 2 with the exception of $\beta \gg 1$ and $\Sigma \ll 1$. When $\bar{\eta}'$ and $\bar{\eta}''$ depend only on material parameters, the first term in the braces in (3.35) is a constant, and the second term is proportional to the vorticity, because the parameter β is the product of the vorticity and the current relaxation time.

The constitutive relation (3.36) is further simplified when the magnetic field is perpendicular to the direction of the vorticity. In this case, the particle angular velocity and the vorticity are in the same direction, $\hat{\boldsymbol{\omega}} \cdot \hat{\boldsymbol{H}}$ and $\hat{\Omega}_H$ are zero, and the constitutive relation is

$$\boldsymbol{\sigma}^p = |\boldsymbol{\omega}|\eta\phi\,\Sigma\{M_I^*(\beta\Omega^*)(2\hat{\boldsymbol{e}}_\perp\hat{\boldsymbol{e}}_\parallel - \hat{\boldsymbol{e}}_\parallel\hat{\boldsymbol{e}}_\perp) + M_R^*(\beta\Omega^*)(\hat{\boldsymbol{e}}_\parallel\hat{\boldsymbol{e}}_\parallel - \hat{\boldsymbol{e}}_\perp\hat{\boldsymbol{e}}_\perp)\}, \qquad (3.36)$$

where Ω^* is the solution of equation (3.6) with $\hat{\boldsymbol{\omega}} \cdot \hat{\boldsymbol{H}} = 0$, $\hat{\Omega}_H = 0$ and $\hat{\Omega}_\omega = 1$:

$$1 - \Omega^* - \Sigma M_I^*(\beta\Omega^*) = 0. \qquad (3.37)$$

4. Conclusions

4.1. *Parameter regimes*

Realistic numerical values of the parameters β and Σ were estimated in Kumaran (2019) for particles made of conducting materials such as copper or aluminium. The parameter β, which is proportional to the square of the particle radius, is $O(1)$ only for millimetre-sized particles at a very high vorticity of 10^3–10^4 s^{-1}. For most practical applications, the parameter β is small and the limit $\beta \ll 1$ is most relevant. However, there are special cases such as ultra-low-resistivity materials and type II superconductors where large values of β can be realised in practice. The parameter Σ is independent of the particle radius, and it is proportional to the square of the magnetic field. The magnetic field H_0 can be varied over a wide range. The value of H_0 for the Earth's magnetic field is about 50 A m^{-1}, but a practically realisable magnetic field of about 1 T results in $H_0 \sim 10^6$ A m^{-1}. Consequently, Σ can be varied over a wide range from 10^{-3} to 10^3 in experiments.

The parameter $\beta\Sigma$ is independent of the fluid vorticity, and the magnitudes of this dimensionless number are estimated as follows. If we consider a suspension of particles of low-resistivity materials such as aluminium and copper, $\varrho \sim 2 \times 10^{-8}$ kg m^3 s^{-3} A^{-2}, suspended in water with viscosity $\eta \sim 10^{-3}$ kg m^{-1} s^{-1}, the parameter $\beta_p\Sigma \sim 3 \times 10^{-3}H_0^2R^2$, where H_0 is the magnetic field with unit A m^{-1} and the radius R is expressed in metres. If the particle size is 10–100 μm, it is easy to access the regimes $\beta_p\Sigma \ll 1$ and $\beta_p\Sigma \gg 1$ by using magnetic field strengths in the range 50–10^6 A m^{-1}. For a thin shell, the functions $\bar{\eta}'$ and $\bar{\eta}''$ depend on the parameter $\beta_s\Sigma = (\mu_0^2H_0^2R^2\delta/8\pi\eta\varrho)$, which is smaller than $\beta_p\Sigma$ by a factor δ, the ratio of the shell thickness and particle radius. In this case, as well, the parameter regimes $\beta_s\Sigma \ll 1$ and $\beta_s\Sigma \gg 1$ are accessible using particles of diameter 10–100 μm and H_0 in the range 50–10^6 A m^{-1}.

For charged particles in a viscous fluid discussed in appendix C, there are two dimensionless parameters: the ratio of magnetic and viscous stress $\Sigma_{ch} = (C_\Omega Q\mu_0H_0/8\pi\eta R)$, which is independent of the fluid vorticity, and the parameter $\beta_{ch} = C_\Omega^2Q^2\mu_0|\boldsymbol{\omega}|/(8\pi)^2\eta R^2)$, which is a linear function of the fluid vorticity but is independent of the magnetic field. The typical surface charge density for colloidal particles is of the order of 10^{-2} C m^{-2} (Fernandez-Barbero *et al.* 1996), resulting in the maximum value of $\Sigma_{ch} \sim 6 \times 10^{-5}$ for particles of diameter 10 μm and magnetic field strength $H_0 = 10^6$ A m^{-1}. However, a charge density as large as 1 C m^{-2} has been reported in magnetic nanoparticles suspended in polar solvents. If such large charge densities can be realised in particles of radius 10 μm, the parameter Σ_{ch} for such particles is $O(6 \times 10^{-3})$ (Brown *et al.* 2013; Campos *et al.* 2017). The parameter β_{ch} is much smaller, about $3 \times 10^{-14}|\boldsymbol{\omega}|$ for particles with diameter 10 μm, charge density 1 C m^{-2} and $H_0 = 10^6$ A m^{-1}, where $\boldsymbol{\omega}$ is expressed in s^{-1}. Therefore, the terms proportional to β_{ch} can be neglected in the particle stress, and only the $O(\Sigma_{ch})$ contributions to the stress coefficients are of relevance. This approximation leads to a simplified constitutive relation, (C 21).

It should be noted that this effect will be difficult to observe in aqueous solutions with ions, due the presence of a counter-ion layer around each particle. When a particle with surface charges rotates, the counter-ion layer also rotates due to the no-slip boundary condition at the surface. If the Debye length is much smaller than the particle radius, the magnetic moment due to particle rotation is nearly balanced by that due to the rotation of the counter-ion layer; the ratio of the difference in the magnetic moment of the two and the moment due to the surface charges is comparable to the ratio of the Debye layer thickness and the particle size. In contrast, in non-polar solvents, there is very little screening, and the Debye layer thickness could be larger than the particle radius (Hsu, Dufresne & Weitz 2005; Waggett, Shafiq & Bartlett 2018). In such cases, it should be possible to observe rheology modification or secondary flow due to the effect of the magnetic field on a charged particle.

4.2. *Particle stress*

Equation (2.4) is the principal result for the particle stress due to a suspension of dipolar particles in an external field. Though consistent with the expression of Batchelor (1970) for the relation between the particle torque and the antisymmetric part of the stress tensor, this expression is more general because it enables calculation of the symmetric particle stress as well. Though this was evaluated for a magnetic dipole in a magnetic field, the same expression applies for an electrical dipole in an electric field if ϵ_0 and E_0 are substituted for μ_0 and H_0, and $\boldsymbol{M}$ is considered the electric dipole moment instead of the magnetic dipole moment. For an isotropic polarisable particle, the electric dipole moment is along

the direction of the electric field, and therefore there is no antisymmetric part for the particle stress. However, particles with a permanent dipole and those with anisotropic polarisability could have an antisymmetric contribution to the particle stress.

4.3. *Magnetic moment*

It is known (Halverson & Cohen 1964; Landau *et al.* 2014) that the component of the magnetic moment along the direction of the angular velocity is zero. An interesting additional result here, (3.11), is that the component of the moment along the vorticity direction is zero for a conducting particle in a linear shear flow in the viscous limit. This appears to be a consequence of the torque balance condition, and this second condition serves to fix the direction of the magnetic moment perpendicular to the angular velocity–vorticity plane where the two are not parallel. In contrast, the magnetic moment for a charged particle does have a component along the vorticity direction, as shown in (C 10). In fact, in the practically realisable limit $\Sigma_{ch} \ll 1$, the particle magnetic moment is primarily along the vorticity direction for a charged particle.

4.4. *Rheology*

At the outset, it is important to note that the particle stress due to the magnetic field is related to the vorticity at the particle centre. This is in contrast to the Einstein calculation for the stress due to a suspension of rigid particles in a fluid, where the particle stress is related to the symmetric traceless part of the rate of deformation tensor. In addition, the stress tensor due to the magnetic field is not symmetric, and therefore the velocity disturbance and secondary flow resulting from a magnetic field will be qualitatively different from that due to a rigid sphere in a linear shear flow.

A general rheological model for the stress in an incompressible fluid consists of three symmetric stress coefficients for the symmetric component of the stress tensor in three perpendicular planes, two normal stress coefficients for the two normal stress differences and three antisymmetric stress coefficients for the antisymmetric part of the stress tensor. In Kumaran (2019), the three antisymmetric stress coefficients were evaluated, and it was shown that there are only two independent coefficients due to the constraint that the particle torque is perpendicular to the magnetic field. This relationship is also evident from (2.6) when the magnetic moment is perpendicular to the vorticity direction. The symmetric traceless part of the stress tensor in (2.5) contains two terms, one of which is linear and the second is quadratic in the particle magnetic moment. Therefore, the symmetric part depends on five functions: $M_{\parallel}$, $M_{\perp}$, $M_{\parallel}^2$, $M_{\perp}^2$ and $M_{\parallel}M_{\perp}$. However, the quadratic term in (2.5) is numerically smaller than the linear contribution.

In the 'linear' approximation (3.35), where the terms quadratic in the magnetic moment are neglected, the eight stress coefficients depend on two functions: $\bar{\eta}'(\beta, \Sigma, \hat{\boldsymbol{\omega}} \cdot \hat{\boldsymbol{H}})$ and $\bar{\eta}''(\beta, \Sigma, \hat{\boldsymbol{\omega}} \cdot \hat{\boldsymbol{H}})$. These functions depend on $\hat{\boldsymbol{\omega}} \cdot \hat{\boldsymbol{H}}$ only for $\Sigma \sim 1$ and $\beta_p \gtrsim 10$ for a uniform particle and $\beta_s \gtrsim 3$ for a thin shell. In all other parameter regimes, the functions $\bar{\eta}'$ and $\bar{\eta}''$ are independent of $\hat{\boldsymbol{\omega}} \cdot \hat{\boldsymbol{H}}$. However, it should be noted that the stress tensor (3.35) does explicitly depend on $\hat{\boldsymbol{\omega}} \cdot \hat{\boldsymbol{H}}$.

For a uniform particle, the functions $\bar{\eta}'(\beta_p, \Sigma)$ and $\bar{\eta}''(\beta_p, \Sigma)$ (figure 4) are only functions of $\beta_p \Sigma$ for $\beta_p \lesssim 3$ for all Σ, and for $\Sigma \gtrsim \sqrt{\beta_p}$ and $\beta_p \gtrsim 3$. For a thin shell, $\bar{\eta}'(\beta_s, \Sigma)$ and $\bar{\eta}''(\beta_s, \Sigma)$ (figure 5) are functions of $\beta_s \Sigma$ for $\beta_s \lesssim 1$ for all Σ, and for $\Sigma \gtrsim (2\beta_s/3)$ and $\beta_s \gtrsim 1$. This constitutes a significant simplification, because the parameter $\beta_p \Sigma$ depends on material properties and the magnetic field, and is independent of the

vorticity. With this simplification, the stress (3.35) has two parts, the first proportional to $|\boldsymbol{\omega}|\bar{\eta}'(\beta\Sigma)$ is a linear function of the vorticity and the second proportional to $|\boldsymbol{\omega}|\beta\bar{\eta}''(\beta\Sigma)$ is proportional to the square of the vorticity, because the parameter β is the product of the vorticity and the current relaxation time. The latter is $O(\beta)$ smaller than the former in the relevant limit $\beta \ll 1$ discussed in § 4.1.

For a unidirectional flow where the velocity is in the x direction and the velocity gradient is in the y direction, the rheology modification is strongest when the magnetic field is parallel to the flow direction, that is, $\hat{\boldsymbol{e}}_\parallel = \boldsymbol{e}_x$ and $\hat{\boldsymbol{e}}_\perp = \boldsymbol{e}_y$. In this case, (3.35) indicates that the eddy current contribution to the viscosity is $2\eta\phi\bar{\eta}'$. The function $\bar{\eta}'$ approaches a maximum value of 1 in the limit of high magnetic field. Therefore, the maximum increment in the viscosity due to the Maxwell stress is $2\eta\phi$; this is in addition to the Einstein increment due to the a rigid particle in a shear flow, $5(\eta\phi)/2$. Of the viscosity increment due to the Maxwell stress, $3(\eta\phi)/2$ is due to the antisymmetric part of the stress tensor and $(\eta\phi)/2$ is due to the symmetric part of the stress tensor.

It is shown in appendix C that analytical solutions can be obtained for the particle angular velocity and stress coefficients for a suspension of charged particles in a shear flow. In this case, the ratio of the magnetic and viscous torques, Σ_{ch}, is independent of the vorticity and the parameter β_{ch} is a linear function of the vorticity. Based on the estimates in § 4.1, the numerical value of β_{ch} is negligible, and only the terms linear in Σ_{ch} could result in a significant rheology modification. The largest contributions to the stress are due to the second symmetric stress coefficient, the second normal stress coefficient and the third antisymmetric stress coefficient; in contrast, these three coefficients provide the smallest contribution to the stress for a suspension of conducting particles. The linear approximation for the stress tensor, (C 21), contains an asymmetric stress in the $\hat{\boldsymbol{\omega}}$–$\hat{\boldsymbol{H}}$ plane, and a normal stress difference between the normal stresses in the vorticity direction and the direction perpendicular to the $\hat{\boldsymbol{\omega}}$–$\hat{\boldsymbol{H}}$ plane.

Declaration of interest

The author reports no conflict of interest.

Appendix A. Calculation of particle stress

Since the particle stress tensor is not symmetric, it is important to specify the convention for calculating the particle stress used here and in Kumaran (2019). In indicial notation, the stress $\sigma_{ij}^{(p)}$ is defined as the force per unit area in the j direction acting on a surface with outward unit normal in the i direction. Using this notation, the force density acting on the fluid in the Navier–Stokes momentum conservation equation, $\nabla \cdot \boldsymbol{\sigma}^p$, is written in indicial notation as $(\partial\sigma_{ij}^{(p)}/\partial x_i)$.

The particle stress in (2.4) is evaluated as follows. Using the notation $\boldsymbol{r} = (\boldsymbol{x} - \boldsymbol{x}_c)$ and $r = |\boldsymbol{x} - \boldsymbol{x}_c|$, the magnetic field (2.1) is expressed in indicial notation as

$$H_i = H_{0i} + \frac{1}{4\pi}\left(\frac{3r_i r_k}{r^5} - \frac{\delta_{ik}}{r^3}\right)M_k. \tag{A 1}$$

The Maxwell stress, (2.2), is

$$
\sigma_{lj}^{M} - \mu_0 \left(H_{0j} H_{0l} - \frac{1}{2} \delta_{jl} H_{0k} H_{0k} \right)
$$

$$
= \frac{\mu_0}{4\pi} \left[H_{0j} \left(\frac{3 r_l r_k}{r^5} - \frac{\delta_{lk}}{r^3} \right) M_k + H_{0l} \left(\frac{3 r_j r_k}{r^5} - \frac{\delta_{jk}}{r^3} \right) M_k \right.
$$

$$
\left. - \delta_{jl} H_{0m} \left(\frac{3 r_m r_k}{r^5} - \frac{\delta_{mk}}{r^3} \right) M_k \right]
$$

$$
+ \frac{\mu_0}{16\pi^2} \left[\left(\frac{3 r_j r_k}{r^5} - \frac{\delta_{jk}}{r^3} \right) \left(\frac{3 r_l r_m}{r^5} - \frac{\delta_{lm}}{r^3} \right) M_k M_m \right.
$$

$$
\left. - \frac{\delta_{jl}}{2} \left(\frac{3 r_p r_k}{r^5} - \frac{\delta_{pk}}{r^3} \right) \left(\frac{3 r_p r_m}{r^5} - \frac{\delta_{pm}}{r^3} \right) M_k M_m \right]. \tag{A 2}
$$

The force moment is

$$
r_i n_l \left(\sigma_{lj}^{M} - \mu_0 \left(H_{0j} H_{0l} - \frac{1}{2} \delta_{jl} H_{0k} H_{0k} \right) \right)
$$

$$
= \frac{\mu_0}{4\pi} \left[H_{0j} \left(\frac{3 r_i r_l^2 r_k}{r^6} - \frac{r_i r_k}{r^4} \right) M_k + H_{0l} \left(\frac{3 r_i r_j r_l r_k}{r^6} - \frac{r_l r_i \delta_{jk}}{r^4} \right) M_k \right.
$$

$$
\left. - \delta_{jl} H_{0m} \left(\frac{3 r_i r_l r_m r_k}{r^6} - \frac{r_i r_l \delta_{mk}}{r^4} \right) M_k \right]
$$

$$
+ \frac{\mu_0}{16\pi^2} \left[\left(\frac{3 r_i r_k r_j r_l}{r^6} - \frac{\delta_{jk} r_i r_l}{r^4} \right) \left(\frac{3 r_l r_m}{r^5} - \frac{\delta_{lm}}{r^3} \right) M_k M_m \right.
$$

$$
\left. - \frac{\delta_{jl} r_i r_l}{2r} \left(\frac{3 r_p r_k}{r^5} - \frac{\delta_{pk}}{r^3} \right) \left(\frac{3 r_p r_m}{r^5} - \frac{\delta_{pm}}{r^3} \right) M_k M_m \right]
$$

$$
= \frac{\mu_0}{4\pi} \left[H_{0j} \left(\frac{3 r_i r_k}{r^4} - \frac{r_i r_k}{r^4} \right) M_k + H_{0l} \left(\frac{3 r_i r_j r_l r_k}{r^6} - \frac{r_l r_i \delta_{jk}}{r^4} \right) M_k \right.
$$

$$
\left. - H_{0m} \left(\frac{3 r_i r_j r_m r_k}{r^6} - \frac{r_j r_i \delta_{mk}}{r^4} \right) M_k \right]
$$

$$
+ \frac{\mu_0}{16\pi^2} \left[\left(\frac{6 r_i r_j r_k r_m}{r^9} - \frac{2 \delta_{jk} r_i r_m}{r^7} \right) M_k M_m \right.
$$

$$
\left. - \frac{r_i r_j}{2r} \left(\frac{3 r_k r_m}{r^8} + \frac{\delta_{km}}{r^6} \right) M_k M_m \right]
$$

$$
= \frac{\mu_0}{4\pi} \left[H_{0j} \left(\frac{2 r_i r_k}{r^4} \right) M_k - H_{0l} M_j \left(\frac{r_l r_i}{r^4} \right) + H_{0k} \left(\frac{r_j r_i}{r^4} \right) M_k \right]
$$

$$
+ \frac{\mu_0}{16\pi^2} \left[\left(\frac{9 r_i r_j r_k r_m}{2 r^9} - \frac{2 \delta_{jk} r_i r_m}{r^7} - \frac{\delta_{km} r_i r_j}{2 r^7} \right) M_k M_m \right]. \tag{A 3}
$$

Using the identities

$$\int_S dS \, r_i r_j = \frac{4\pi r^4 \delta_{ij}}{3}, \\ \int_S dS \, r_i r_j r_k r_m = \frac{4\pi r^6 (\delta_{ij}\delta_{km} + \delta_{ik}\delta_{jm} + \delta_{im}\delta_{jk})}{15}, \quad \left.\right\} \tag{A 4}$$

the integral of the force moment over the surface of the sphere is

$$\int_S dS \, r_i n_l \left(\sigma_{jl}^M - \mu_0 \left(H_{0j}H_{0l} - \frac{1}{2}\delta_{jl}H_{0k}H_{0k} \right) \right) \\ = \mu_0 \left[\left(\frac{2M_i H_{0j}}{3} - \frac{H_{0i}M_j}{3} + \frac{\delta_{ij}H_{0k}M_k}{3} \right) + \frac{1}{60\pi R^3} \left(-M_i M_j + 2\delta_{ij}M_k^2 \right) \right]. \tag{A 5}$$

The particle stress is

$$\sigma_{ij}^{(p)} = \frac{\phi}{(4\pi R^3/3)} \int_S dS \, \sigma_{jl}^M n_l r_i \\ = \mu_0 \phi \left[\left(\frac{M_i H_{0j}}{2\pi R^3} - \frac{H_{0i}M_j}{4\pi R^3} + \frac{\delta_{ij}H_{0k}M_k}{4\pi R^3} \right) + \frac{1}{80\pi^2 R^6} \left(-M_i M_j + 2\delta_{ij}M_k^2 \right) \right]. \tag{A 6}$$

The particle stress can be separated into the its symmetric and antisymmetric parts:

$$\sigma_{sij}^{(p)} = \frac{1}{2}(\sigma_{ij}^{(p)} + \sigma_{ji}^{(p)}) \\ = \frac{\mu_0 \phi (M_i H_{0j} + M_j H_{0i} + 2\delta_{ij}M_k H_{0k})}{8\pi R^3} \\ + \frac{\mu_0 \phi (-M_i M_j + 2\delta_{ij}M_k^2)}{80\pi^2 R^6}, \tag{A 7}$$

$$\sigma_{aij}^{(p)} = \frac{1}{2}(\sigma_{ij}^{(p)} - \sigma_{ji}^{(p)}) \\ = \frac{\mu_0 \phi}{(4\pi R^3/3)} \left(\frac{M_i H_{0j} - H_{0i}M_j}{2} \right). \tag{A 8}$$

From (1.1), the antisymmetric part of the stress tensor can also be obtained from the torque on the particle:

$$\sigma_{aij}^{(p)} = \frac{1}{2} \frac{\phi}{(4\pi R^3/3)} \epsilon_{ijk} L_k, \tag{A 9}$$

where $L_k = \epsilon_{klm}\mu_0 M_l H_{0m}$ is the torque exerted on a particle and ϵ_{ijk} is the Levi-Civita antisymmetric tensor in indicial notation.

Appendix B. Particle magnetic moment

The scaled magnetic moments M_R^* and M_I^* were calculated in Halverson & Cohen (1964) using phaser algebra and in Kumaran (2019) using a simpler vector notation. For a uniform

	Uniform particle		Thin shell	
	$\beta_p\Omega^* \ll 1$	$\beta_p\Omega^* \gg 1$	$\beta_s\Omega^* \ll 1$	$\beta_s\Omega^* \gg 1$
$M_R(\beta\Omega^*)$	$-((\beta_p\Omega^*)^2/315)$	$-(1/2)$	$-((\beta_s\Omega^*)^2/18)$	$-(1/2)$
$M_I(\beta\Omega^*)$	$(\beta_p\Omega^*/30)$	$(3/2\sqrt{2\beta_p\Omega^*})$	$(\beta_s\Omega^*/6)$	$(3/2\beta_s\Omega^*)$

TABLE 3. The asymptotic behaviour of the functions $M_R^*(\beta\Omega^*)$ (equations (B 1) and (B 3)) and $M_I^*(\beta\Omega^*)$ (equations (B 2) and (B 4)) in the limits $\beta\Omega^* \ll 1$ and $\beta\Omega^* \gg 1$.

particle of radius R, the scaled magnetic moments M_R^* and M_I^* are

$$M_R^* = -\frac{1}{2} + \frac{3}{2\sqrt{2\beta_p\Omega^*}} \frac{\sinh{(\sqrt{2\beta_p\Omega^*})} - \sin{(\sqrt{2\beta_p\Omega^*})}}{\cosh{(\sqrt{2\beta_p\Omega^*})} - \cos{(\sqrt{2\beta_p\Omega^*})}}, \tag{B 1}$$

$$M_I^* = -\frac{3}{2\beta_p\Omega^*} + \frac{3}{2\sqrt{2\beta_p\Omega^*}} \frac{\sinh{(\sqrt{2\beta_p\Omega^*})} + \sin{(\sqrt{2\beta_p\Omega^*})}}{\cosh{(\sqrt{2\beta_p\Omega^*})} - \cos{(\sqrt{2\beta_p\Omega^*})}}, \tag{B 2}$$

where $\Omega^* = |\boldsymbol{\Omega}/(|\boldsymbol{\omega}/2|)|$ is the scaled angular velocity, $\beta_p = (|\boldsymbol{\omega}|\mu_0 R^2/2\varrho)$, $\boldsymbol{\omega}$ is the fluid vorticity at the particle centre, R is the particle radius, μ_0 is the magnetic permittivity and ϱ is the electrical resistivity. For a thin shell of radius R and thickness δR with $\delta \ll 1$, the scaled magnetic moments are

$$M_R^* = \frac{-\beta_s^2\Omega^{*2}}{2(9 + \beta_s^2\Omega^{*2})}, \tag{B 3}$$

$$M_I^* = \frac{3\beta_s\Omega^*}{2(9 + \beta_s^2\Omega^{*2})}, \tag{B 4}$$

where $\beta_s = (|\boldsymbol{\omega}|\mu_0 R^2\delta/2\varrho)$. The limiting behaviours of the magnetic moments for $\beta\Omega^* \ll 1$ and $\beta\Omega^* \gg 1$ are provided in table 3.

Appendix C. Charged particle

The magnetic dipole moment $\boldsymbol{M}$ induced in a charged sphere of radius R rotating with angular velocity $\boldsymbol{\Omega}$ is

$$\boldsymbol{M} = \frac{1}{2} \int_V dV \, \boldsymbol{x} \times (\varrho_c \boldsymbol{v}), \tag{C 1}$$

where ϱ_c is the charge density, $\boldsymbol{v}$ is the velocity and $\boldsymbol{x}$ is the distance from the centre of the sphere. For a rotating sphere, the velocity is $\boldsymbol{v} = \boldsymbol{\Omega} \cdot \boldsymbol{x}$ and the magnetic moment is

$$\boldsymbol{M} = \frac{1}{2} \int_V dV \, \boldsymbol{x} \times (\varrho_c \boldsymbol{\Omega} \times \boldsymbol{x}). \tag{C 2}$$

If the particle is spherically symmetric, that is, the charge density $\varrho_c(r)$ depends only on the distance r from the centre of the sphere, the magnetic moment is

$$\boldsymbol{M} = \frac{4}{3}\pi\boldsymbol{\Omega} \int_{R_i}^{R_o} r^4 \, dr \, \varrho_c(r). \tag{C 3}$$

The magnetic moment can then be written as

$$\boldsymbol{M} = C_\Omega \boldsymbol{\Omega} R^2 Q, \tag{C 4}$$

where Q is the total particle charge and C_Ω is a constant which depends on the radial charge distribution. For example, if the charge density is uniform throughout the particle volume, $\varrho_c = Q/(4\pi R^3/3)$, then $C_\Omega = 1/5$. If the charges are located only on the surface of the particle, $\varrho_c = (Q/4\pi R^2)\delta(r - R)$, then $C_\Omega = 1/3$.

The hydrodynamic and magnetic torques on a particle in a shear flow, $\boldsymbol{T}^h$ and $\boldsymbol{T}^m$, are

$$\boldsymbol{T}^h = 4\pi\eta(\boldsymbol{\omega} - 2\boldsymbol{\Omega}), \tag{C 5}$$

$$\boldsymbol{T}^m = \mu_0 \boldsymbol{M} \times \boldsymbol{H}_0 = (C_\Omega \boldsymbol{\Omega} Q R^2 \mu_0) \times \boldsymbol{H}_0, \tag{C 6}$$

where $\boldsymbol{\omega}$ is the fluid vorticity at the particle location determined in the absence of the particle. In the limit of low Reynolds number, the total torque on a particle is zero, and the torque balance equation is

$$4\pi\eta R^3(\boldsymbol{\omega} - 2\boldsymbol{\Omega}) + C_\Omega Q R^2 \mu_0 H_0(\boldsymbol{\Omega} \times \hat{\boldsymbol{H}}) = 0. \tag{C 7}$$

The above equation is divided by $8\pi\eta R^3$ to obtain a relation between the angular velocity, vorticity and the magnetic field vector:

$$\tfrac{1}{2}\boldsymbol{\omega} = \boldsymbol{\Omega} - \Sigma_{ch}(\boldsymbol{\Omega} \times \hat{\boldsymbol{H}}), \tag{C 8}$$

where $\Sigma_{ch} = (C_\Omega Q \mu_0 H_0/8\pi\eta R)$ is a dimensionless number which is a ratio of the magnetic and viscous torques. Equation (C 8) can be solved to obtain the angular velocity:

$$\boldsymbol{\Omega} = \frac{\boldsymbol{\omega} + \Sigma_{ch}\boldsymbol{\omega} \times \hat{\boldsymbol{H}} + \Sigma_{ch}^2 \hat{\boldsymbol{H}}(\boldsymbol{\omega} \cdot \hat{\boldsymbol{H}})}{2(1 + \Sigma_{ch}^2)}. \tag{C 9}$$

Substituting the angular velocity in (C 4), the components of the particle magnetic moment $(\hat{\boldsymbol{e}}_\parallel, \hat{\boldsymbol{e}}_\perp, \hat{\boldsymbol{\omega}})$ coordinate system are

$$M_\omega = \frac{C_\Omega Q R^2 |\boldsymbol{\omega}|(1 + \Sigma_{ch}^2(\hat{\boldsymbol{\omega}} \cdot \hat{\boldsymbol{H}})^2)}{2(1 + \Sigma_{ch}^2)}, \tag{C 10}$$

$$M_\parallel = \frac{C_\Omega Q R^2 |\boldsymbol{\omega}| \Sigma_{ch}^2(\hat{\boldsymbol{\omega}} \cdot \hat{\boldsymbol{H}})\sqrt{1 - (\hat{\boldsymbol{\omega}} \cdot \hat{\boldsymbol{H}})^2}}{2(1 + \Sigma_{ch}^2)}, \tag{C 11}$$

$$M_\perp = \frac{C_\Omega Q R^2 |\boldsymbol{\omega}| \Sigma_{ch}\sqrt{1 - (\hat{\boldsymbol{\omega}} \cdot \hat{\boldsymbol{H}})^2}}{2(1 + \Sigma_{ch}^2)}. \tag{C 12}$$

From (2.5), (2.6) and (3.16), the symmetric, normal and antisymmetric stress coefficients are

$$\eta_s^{(1)} = \frac{\eta\phi \Sigma_{ch}^2(1 - (\hat{\boldsymbol{\omega}} \cdot \hat{\boldsymbol{H}})^2)}{2(1 + \Sigma_{ch}^2)} - \frac{\eta\phi \Sigma_{ch}^3 \beta_{ch}\hat{\boldsymbol{\omega}} \cdot \hat{\boldsymbol{H}}(1 - (\hat{\boldsymbol{\omega}} \cdot \hat{\boldsymbol{H}})^2)}{5(1 + \Sigma_{ch}^2)^2}, \tag{C 13}$$

$$\eta_s^{(2)} = \frac{\eta \phi \Sigma_{ch}^2 \hat{\boldsymbol{\omega}} \cdot \hat{\boldsymbol{H}} \sqrt{1 - (\hat{\boldsymbol{\omega}} \cdot \hat{\boldsymbol{H}})^2}}{2(1 + \Sigma_{ch}^2)}$$
$$- \frac{\eta \phi \Sigma_{ch} \beta_{ch}(1 + \Sigma_{ch}^2(\hat{\boldsymbol{\omega}} \cdot \hat{\boldsymbol{H}})^2)\sqrt{1 - (\hat{\boldsymbol{\omega}} \cdot \hat{\boldsymbol{H}})^2}}{5(1 + \Sigma_{ch}^2)^2}, \tag{C 14}$$

$$\eta_s^{(3)} = \frac{\eta \phi \Sigma_{ch}(1 + 2\Sigma_{ch}^2(\hat{\boldsymbol{\omega}} \cdot \hat{\boldsymbol{H}})^2)\sqrt{1 - (\hat{\boldsymbol{\omega}} \cdot \hat{\boldsymbol{H}})^2}}{2(1 + \Sigma_{ch}^2)}$$
$$- \frac{\eta \phi \Sigma_{ch}^2 \beta_{ch}(1 + \Sigma_{ch}^2(\hat{\boldsymbol{\omega}} \cdot \hat{\boldsymbol{H}})^2)(\hat{\boldsymbol{\omega}} \cdot \hat{\boldsymbol{H}})\sqrt{1 - (\hat{\boldsymbol{\omega}} \cdot \hat{\boldsymbol{H}})^2}}{5(1 + \Sigma_{ch}^2)^2}, \tag{C 15}$$

$$\eta_n^{(1)} = \frac{\eta \phi \Sigma_{ch}^3 \hat{\boldsymbol{\omega}} \cdot \hat{\boldsymbol{H}}(1 - (\hat{\boldsymbol{\omega}} \cdot \hat{\boldsymbol{H}})^2)}{(1 + \Sigma_{ch}^2)}$$
$$+ \frac{\eta \phi \Sigma_{ch}^2 \beta_{ch}(1 - \Sigma_{ch}^2(\hat{\boldsymbol{\omega}} \cdot \hat{\boldsymbol{H}})^2)(1 - (\hat{\boldsymbol{\omega}} \cdot \hat{\boldsymbol{H}})^2)}{5(1 + \Sigma_{ch}^2)^2}, \tag{C 16}$$

$$\eta_n^{(2)} = -\frac{\eta \phi \Sigma_{ch} \hat{\boldsymbol{\omega}} \cdot \hat{\boldsymbol{H}}(1 + \Sigma_{ch}^2(\hat{\boldsymbol{\omega}} \cdot \hat{\boldsymbol{H}})^2)}{(1 + \Sigma_{ch}^2)}$$
$$+ \frac{\eta \phi \beta_{ch}(1 - \Sigma_{ch}^2 + 3\Sigma_{ch}^2(\hat{\boldsymbol{\omega}} \cdot \hat{\boldsymbol{H}})^2 + \Sigma_{ch}^4(\hat{\boldsymbol{\omega}} \cdot \hat{\boldsymbol{H}})^4)}{5(1 + \Sigma_{ch}^2)^2}, \tag{C 17}$$

$$\eta_a^{(1)} = -\frac{3\eta \phi \Sigma_{ch}^2(1 - (\hat{\boldsymbol{\omega}} \cdot \hat{\boldsymbol{H}})^2)}{2(1 + \Sigma_{ch}^2)}, \tag{C 18}$$

$$\eta_a^{(2)} = \frac{3\eta \phi \Sigma_{ch}^2 \hat{\boldsymbol{\omega}} \cdot \hat{\boldsymbol{H}} \sqrt{1 - (\hat{\boldsymbol{\omega}} \cdot \hat{\boldsymbol{H}})^2)}}{2(1 + \Sigma_{ch}^2)}, \tag{C 19}$$

$$\eta_a^{(3)} = \frac{3\eta \phi \Sigma_{ch} \sqrt{1 - (\hat{\boldsymbol{\omega}} \cdot \hat{\boldsymbol{H}})^2}}{2(1 + \Sigma_{ch}^2)}, \tag{C 20}$$

where $\beta_{ch} = (C_\Omega^2 Q^2 \mu_0 |\boldsymbol{\omega}|/(8\pi)^2 \eta R^2)$ is the ratio of the vorticity and the charge relaxation time. The terms proportional to β_{ch} on the right-hand sides in (C 13)–(C 17) are a consequence of the term that is quadratic in the magnetic moment on the right-hand side in (2.5).

As discussed in § 4.1, the value of the parameter Σ_{ch} is numerically small in practical applications. Consequently, the $O(\Sigma_{ch})$ terms are the largest contributions to the stress tensor for a suspension of charged particles in a magnetic field. From (C 13)–(C 20),

the $O(\Sigma_{ch})$ terms in the third symmetric stress coefficient $\eta_s^{(3)}$, the second normal stress coefficient $\eta_n^{(2)}$ and the third antisymmetric stress coefficient $\eta_a^{(3)}$ are the largest corrections to the stress tensor. This is in contrast to the stress tensor for conducting particles calculated in § 3.2, where the coefficients $\eta_s^{(1)}$, $\eta_s^{(3)}$, $\eta_n^{(1)}$, $\eta_a^{(1)}$ and $\eta_a^{(2)}$, which are proportional to $\bar{\eta}'(\beta, \Sigma)$, are much larger in magnitude than $\eta_s^{(2)}$, $\eta_n^{(2)}$ and $\eta_a^{(3)}$, which are proportional to $\bar{\eta}''(\beta, \Sigma)$. The $O(\Sigma_{ch})$ contribution to the stress for conducting particle is, in the $\hat{\boldsymbol{\omega}}$–$\hat{\boldsymbol{e}}_\perp$ plane, given by

$$\boldsymbol{\sigma}^p = \eta \phi \Sigma_{ch} |\boldsymbol{\omega}| [\sqrt{1 - (\hat{\boldsymbol{\omega}} \cdot \hat{H})^2}(2\hat{\boldsymbol{\omega}}\hat{\boldsymbol{e}}_\parallel - \hat{\boldsymbol{e}}_\parallel\hat{\boldsymbol{\omega}}) + (\hat{\boldsymbol{\omega}} \cdot \hat{H})(\hat{\boldsymbol{\omega}}\hat{\boldsymbol{\omega}} - \hat{\boldsymbol{e}}_\perp\hat{\boldsymbol{e}}_\perp)]. \tag{C 21}$$

REFERENCES

ALMOG, Y. & FRANKEL, I. 1995 The motion of axisymmetric dipolar particles in a homogeneous shear flow. *J. Fluid Mech.* **289**, 243–261.

ANUPAMA, A. V., KUMARAN, V. & SAHOO, B. 2018 Magnetorheological fluids containing rod-shaped lithium-zinc ferrite particles: the steady-state shear response. *Soft Matt.* **14**, 5407–5419.

BATCHELOR, G. K. 1970 The stress in a suspension of force-free particles. *J. Fluid Mech.* **41**, 545–570.

BOLCATO, R., ETAY, J., FAUTRELLE, Y. & MOFFATT, H. K. 1993 Electromagnetic billiards. *Phys. Fluids* A **5**, 1852–1853.

BROWN, M. A., DUYCKAERTS, N., REDONDO, A. B., JORDAN, I., NOLTING, F., KLEIBERT, A., AMMANN, M., WORNER, H. J., VAN BOKHOVEN, J. A. & ABBAS, Z. 2013 Effect of surface charge density on the affinity of oxide nanoparticles for the vapor-water interface. *Langmuir* **29** (16), 5023–5029.

CAMPOS, A. F. C., DE MEDEIROS, W. C., AQUINO, R. & DEPEYROT, J. 2017 Surface charge density determination in water based magnetic colloids: a comparative study. *J. Mater. Res.* **20**, 1729–1734.

CHAVES, A., ZAHN, M. & RINALDI, C. 2008 Spin-up flow of ferrofluids: asymptotoic theory and experimental measurements. *Phys. Fluids* **20**, 053102.

CONDIFF, D. W. & DAHLER, J. S. 1964 Fluid mechanical aspects of antisymmetric stress. *Phys. Fluids* **7**, 842–854.

DAHLER, J. S. & SCRIVEN, L. E. 1963 Theory of structured continua. I. General consideration of angular momentum and polarization. *Proc. R. Soc. Lond.* A **275**, 504–527.

FENG, S., GRAHAM, A. L., ABBOTT, J. R. & BRENNER, H. 2006 Antisymmetric stresses in suspensions: vortex viscosity and energy dissipation. *J. Fluid Mech.* **563**, 97–122.

FERNANDEZ-BARBERO, A., CABRERIZO-VILCHEZ, M., MARTINEZ-GARCIA, R. & Hidalgo-Alvarez, R. 1996 Effect of the particle surface charge density on the colloidal aggregation mechanism. *Phys. Rev.* E **53**, 4981–4989.

GOLDSTEIN, H. 1989 *Clasical Mechanics*. Narosa Publishing House, chap. 4.

HALVERSON, R. P. & COHEN, H. 1964 Torque on a spinning hollow sphere in a uniform magnetic field. *IEEE Trans. Aerosp. Navig. Electron.* **ANE-11**, 118–122.

HSU, M. F., DUFRESNE, E. R. & WEITZ, D. A. 2005 Charge stabilization in nonpolar solvents. *Langmuir* **21**, 4881–4887.

JANSONS, K. M. 1983 Determination of the constitutive equations for a magnetic fluid. *J. Fluid Mech.* **137**, 187–216.

KLINGENBERG, D. J. 2001 Magnetorheology: applications and challenges. *AIChE J.* **47**, 246–249.

KLINGENBERG, D. J. & ZUKOSKI, C. F. 1990 Studies on the steady-shear behavior of electrorheological suspensions. *Langmuir* **6**, 15–24.

KUMARAN, V. 2019 Rheology of a suspension of conducting particles in a magnetic field. *J. Fluid Mech.* **871**, 139–185.

KUMARAN, V. 2020 Bifurcations in the dynamics of a dipolar spheroid in a shear flow subjected to an external field. *Phys. Rev. Fluids* **5**, 033701.

KUZHIR, P., LOPEZ-LOPEZ, M. T. & BOSSIS, G. 2009 Magnetorheology of fiber suspensions. II. Theory. *J. Rheol.* **53**, 127–151.

LANDAU, L. D., LIFSHITZ, E. M. & PITAEVSKII, L. P. 2014 *Electrodynamics of Continuous Media*. Butterworth-Heinemann.

LOPEZ-LOPEZ, M. T., KUZHIR, P. & BOSSIS, G. 2009 Magnetorheology of fiber suspensions. I. Experimental. *J. Rheol.* **53**, 115–126.

MINDLIN, R. & TIERSTEN, H. 1962 Effects of couple-stresses in linear elasticity. *Arch. Rat. Mech. Anal.* **11**, 415–448.

MOFFAT, H. K. 1990 On the behaviour of a suspension of conducting particles subjected to a time-periodic magnetic field. *J. Fluid Mech.* **218**, 509–529.

MOSKOWITZ, R. & ROSENSWEIG, R. E. 1967 Nonmechanical torque-driven flow of a ferromagnetic fluid by an electromagnetic field. *Appl. Phys. Lett.* **11**, 301–303.

RINALDI, C. & ZAHN, M. 2002 Effects of spin viscosity on ferrofluid flow profiles in alternating and rotating magnetic fields. *Phys. Fluids* **14**, 2847.

ROSENSWEIG, R. E. 2000 Continuum equations for magnetic and dielectric fluids with internal rotations. *J. Chem. Phys.* **121**, 1228.

SHERMAN, S. G., BECNEL, A. C. & WERELEY, N. M. 2015 Relating mason number to bingham number in magnetorheological fluids. *J. Magn. Magn. Mater.* **380**, 98–104.

SOBECKI, C. A., ZHANG, J., ZHANG, Y. & WANG, C. 2018 Dynamics of paramagnetic and ferromagnetic ellipsoidal particles in shear flow under a uniform magnetic field. *Phys. Rev. Fluids* **3**, 084201.

STOKES, V. K. 1966 Couple stresses in fluids. *Phys. Fluids* **9**, 1709–1715.

TRUESDELL, C. & TOUPIN, R. A. 1960 The classical field theories. In *Handbuch der Physik* (ed. S. Flugge), pp. 545–609. Springer.

VAGBERG, D. & TIGHE, B. P. 2017 On the apparent yield stress in non-Brownian magnetorheological fluids. *Soft Matt.* **13**, 7207–7221.

DE VICENTE, J., KLINGENBERG, D. J. & HIDALGO-ALVAREZ, R. 2011 Magnetorheological fluids: a review. *Soft Matt.* **7**, 3701–3710.

WAGGETT, F., SHAFIQ, M. D. & BARTLETT, P. 2018 Failure of Debye-Hückel screening in low-charge colloidal suspensions. *Colloids Interfaces* **2**, 51.

WANG, W. & PROSPERETTI, A. 2001 Flow of spatially non-uniform suspensions. Part III: closure relations for porous media and spinning particles. *Intl J. Multiphase Flow* **27**, 1627–1653.

ZAITSEV, V. M. & SHLIOMIS, M. I. 1969 Entrainment of ferromagnetic suspension by a rotating field. *J. Appl. Mech. Tech. Phys.* **10**, 696–700.